Department of Precision and Microsystems Engineering

Towards Multi Shape-Morphing Structures

Jasper Pels

Report no : 2023.027
Coach : Dr. ir. G. Radaelli
Professor : Prof. dr. ir. J. L Herder
Specialisation : MSD
Type of report : Thesis report
Date : 11-05-2023

Towards Multi Shape-Morphing Structures

Jasper Pels

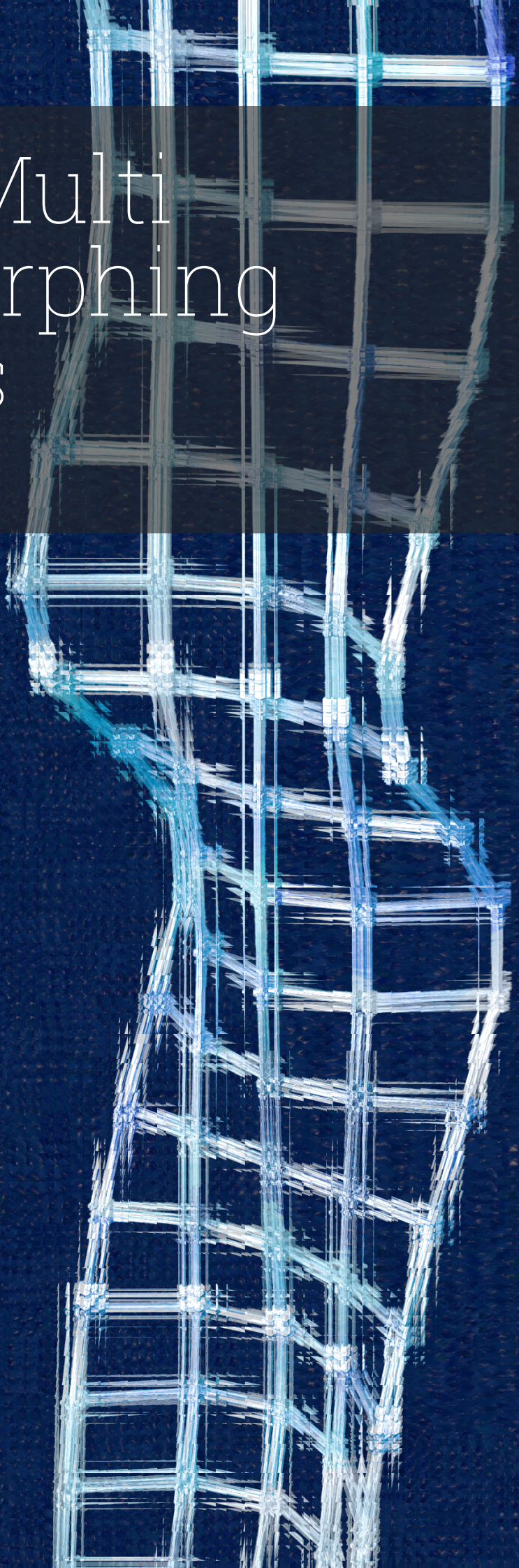

Delft University of Technology

TU Delft

Towards Multi Shape-Morphing Structures

by

Jasper Pels

Student number: 4610539
Thesis committee: Prof. dr. ir. J. L Herder, TU Delft, supervisor
Dr. ir. G. Radaelli, TU Delft, daily supervisor
Ir. A. Amoozandeh Nobaveh, TU Delft, daily supervisor
Ir. S. Filius, TU Delft, thesis committee member
Project Duration: March, 2022 - June, 2023

TU Delft

Preface

This thesis presents a novel design method for acquiring multi shape-morphing behavior in structures, which is a topic of great interest in the field of mechanical engineering. This project was carried out as a part of acquiring my masters degree at Delft University of Technology, where I had the opportunity to explore a new and exciting research area.

By doing this research project, I had an opportunity to apply theoretical concepts to real-world problems, which allowed me to gain hands-on experience in designing and developing multi shape morphing structures such as exoskeletons. It has also helped me to develop skills in conducting experiments, analyzing results, and presenting findings in an effective way.

I would like to express my gratitude to my supervisors Dr. ir. G. Radaelli, Prof. dr. ir. J. L Herder and Ir. A. Amoozandeh Nobaveh at TU Delft for their guidance, support, and valuable feedback throughout this project. Their expertise and knowledge have been invaluable in shaping my ideas and approaches. I would also like to thank my girlfriend, family and friends for their encouragement and motivation.

I hope that this thesis will inspire and motivate future researchers to explore new avenues in designing structures with advanced shape morphing capabilities.

Jasper Pels
Delft, May 2023

Summary

Structures that are capable of changing their shape in a predetermined manner can be found in various domains. For example, in nature, the *Mimosa Pudica* plant adapts its shape to the day and night cycle. In architecture, hygroscopic materials are utilized to allow building facades to adapt to changing weather conditions. In engineering, shape-changing components are deployed to allow for multiple working conditions such as in adaptive turbine blades and morphing aircraft wings. This phenomenon is called shape morphing. The aim of this research is to enhance conventional shape morphing, which involves transitioning between an initial and final shape, by introducing intermediate shapes to enable multi-shape morphing. This paper focuses on the application of this concept in the design of lightweight, flush exoskeletons.

To achieve multi-shape morphing, a novel design method and structure model are presented. The shape of this mechanical structure is influenced at multiple locations by altering its curvature and the Y-axis offset within specific bounds. By comparing structural node locations with objective shape nodes, an assessment of multi shape morphing capability can be made. This measure of performance is used in an optimization based design method consisting of a random search to acquire a representative sample of the design space followed by a minimization of a set of best performing designs, to find designs an approximation of the best possible solutions.

To ensure the physical feasibility of this multi-shape morphing behavior, physical models are produced and their deformation behavior is evaluated under appropriate boundary conditions. Additionally, a sensitivity analysis is conducted on relevant designs to analyze the relative importance of the geometric design variables.

It was found that when influencing the structural shape at a sufficient number of points, not only shape morphing but multi shape morphing can be achieved. When the provided shapes are relatively simple, a low error between the provided and structural shapes can be achieved. However, as complexity increases, certain limits become apparent. Due to the numerous geometric parameters involved, comprehending the mechanical behavior of the structure can be challenging. Therefore, the main advantage of the proposed design method is that without vast knowledge of the influence of geometric parameters of the structure, a representative set of designs can be generated for a given set of objective shapes.

Further research into the phenomena of multi shape morphing could improve upon the current paradigm of mechanical structures by allowing mechanisms to be more functionally capable in deformation or lower in weight due to replacement of multiple components by a single, more capable component.

Contents

From Two Shapes to Many: A literature review on Shape Morphing in Solids, Metamaterials and Origami Structures

J.H. Pels
Delft University of Technology, Delft – Zuid Holland, The Netherlands

***Abstract*—A literature study is presented on shape morphing methods and strategies in order to provide an overview, evaluation and interpretation on the current advancements in the field. Firstly, literature is analysed based on relevance criteria. It is then classified based on the underlying evaluation methods such as FEM, IFEM, PRBM and analytical methods, as well as on structure types such as solids, metamaterials and origami structures. Shape morphing methods and strategies in the literature in these categories are then evaluated based on how many distinct shapes they are able to follow during their deformation path. The results of this study show that while a lot of research has been conducted on structures that are able to morph in shape between two shapes, the amount of research conducted on shape morphing strategies and methods that go beyond this amount is still relatively small, which be attributed to bottlenecks that arise due to the added complexity and increased computational cost as well as material limitations and the novelty of the research field.**

***Index Terms*—shape morphing, metamaterials, origami structures, inverse finite element method**

I. INTRODUCTION

The demand for building better functioning components in industries such as energy, high-tech and space is rapidly increasing. For example, in the high-tech industry, the growing demand for semiconductor chips is driving the need to increase the performance and throughput of the machines that are used to produce these chips. In order to increase the precision, reliability or decrease footprint of a mechanism, engineers are compelled to explore novel techniques to further improve the performance of their designs. Conventionally used Rigid Body Mechanisms that rely on stiff trusses and hinges have been studied for centuries, and these mechanisms are often bottle necked by their weight, reliability or lubrication requirements [1]. Research into new structures such as compliant mechanisms [2]–[4], metamaterials [5], [6] and origami structures [7] that exploit their unique characteristics to outperform conventional mechanisms is gaining traction in recent decades. Characteristics such as compliance [8], auxeticy [9], bi- or multistability [10] or reconfigurability [11] could allow mechanisms to decrease in weight, or improve the functionality of a component by allowing new features that have not been explored. One such characteristic being researched in recent decades is the shape of a mechanism over its full deformation range. This predetermined change in shape during functioning is called Shape Morphing. Shape morphing is *the capability of a structure to change its shape while performing a specific task in order to improve its characteristics or enable new capabilities*. Shape morphing structures can be found in nature [12], architecture [13] and in engineering fields such as aeronautic [14], automobile [15] and architectural engineering [16].

While much research has been conducted on the classification and nomenclature of compliant mechanisms [17] in order to create a basis for compliant design, as well as on the design of shape morphing structures [18] which aided in the following of a single or two shapes, shape morphing structures that are able to morph into multiple distinct provided shapes during their deformation path still remain as a challenge for engineers due to physical limitations, added complexity or the absence of knowledge. Due to this absence of knowledge, this paper aims to present the advancements in the field of shape morphing by reviewing used methods and strategies. Providing a structure with the ability to follow multiple shapes can allow for a larger range of motion or the replacement of multiple components by a single more capable one. This makes more research into this field desirable in order to enable the next paradigm of efficient machines.

The purpose of this literature review is to provide an analysis of relevant literature, a classification of this literature based on the underlying evaluation methods and structure type, and an evaluation of the presented methods and strategies to design a structure that is able to morph into multiple distinct shapes during its deformation path.

In the next chapter, the methodology for this literature report is explained. After this, the results of the literature research are presented and elaborated on. Finally, the results are discussed and interpreted.

II. METHODOLOGY

In this section the method of searching, selection, categorisation and evaluation of literature is explained.

A. CATEGORISATION AND EVALUATION OF LITERATURE

Due to the wide scope of available literature in the field of shape morphing structures, it is necessary to limit the inclusion of research in this literature review based on relevance to the main subject. Commonly used structure types in shape morphing literature are solids, metamaterials and origami structures.

The most used evaluation methods for these structures are analytical methods, Pseudo Rigid Body Model, Finite Element Method and Inverse Finite Element Method.

The conducted procedure for generating literature is described in this chapter. Firstly, literature is found by using the search engines of Google Scholar and Scopus. This literature is selected based on given procedure, thereafter categorized and evaluated.

A categorization of the used search terms to find literature is given in table I. The search process is divided in three levels of detail indicated by $1, 2, 3$. For general shape morphing literature, a single or multiple core terms from 1 were combined and used as a search query. When research was focused on a certain evaluation method or structure type, single or multiple terms from 1 were combined with single or multiple terms from 2. For finding more specific literature, single or multiple additional terms from 3 were used in combination with single or multiple terms from 1, 2 or 1 and 2.

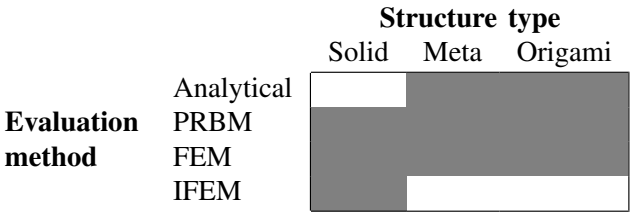

Fig. 1: Literature categorization by evaluation method and structure type, with grey cells representing the presence of literature and white cells representing the absence of literature.

The selection procedure is conducted by assessing whether a described structure is able to morph in shape between at least two distinct shapes and on of the methods from fig. 1 was used to evaluate the structure. It is only relevant to look at structures that have at least two distinct shapes, since this is the minimum requirement for shape morphing. Therefore any intermediary shapes that are not given as a requirement do not count as distinct shapes.

Commonly used structure types found in shape morphing literature and commonly used evaluation methods for these structures are stated in fig. 1 to create a category grid. Grey cells represent the presence of literature and white cells representing the absence of literature. The structure types solids, metamaterials and origami structures given in fig. 1 are defined by their individual commonly exhibited method of shape morphing. Where solids usually deform continuously, metamaterials and origami structures may present characteristics such as bi- or multistability or reconfigurability respectively. These structure types are chosen because they represent commonly found shape morphing mechanisms in a clear manner. When overlap in characteristics occurs between these structure types, the best representing structure type is chosen based its characteristics. The evaluation methods are chosen such that they represent the commonly used evaluation methods for these given structure types. The use of analytical methods means that an analytical procedure was used for evaluation of the shape morphing structure. The Pseudo-Rigid Body Model is a commonly used approximation technique for modeling compliant flexures or mechanisms. The use of FEM and IFEM represent the use of numerical procedures. Each of these structure types combined with their respective evaluation methods are explained more in-depth in their respective chapter in section III.

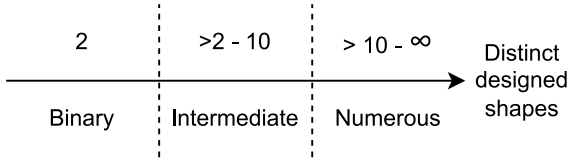

Fig. 2: Shape morphing performance categories based on distinct shape following capability.

The evaluation procedure is based on the ability of the structure or method to follow or design for distinct shapes during its deformation path and can be seen in fig. 2. Three classes are presented within this evaluation system. *Binary* corresponds to two distinct shapes, the second interval is called *Intermediate* and covers $> 2 - 10$ distinct shapes, the last interval covers > 10 distinct shapes and is called *Numerous*. Continuous morphing structures with no clear begin of end state will be classified as *Binary* and thought of as having a discrete initial and end shape unless other distinct intermediate shapes are required by the designer. This phenomena can for example be seen in structures that continuously morph between an contracted and uncontracted state where only the initial and final shape are designed. These structures are able to morph into more than two shapes, however the set of shapes is representative of a range with a beginning and an end and thus is analogous to *Binary* shape morphing.

B. CHAPTER LAYOUT

At the start of each section in the following chapter, the theoretical basis for an evaluation method as used with the structure type is given for each section (corresponding to a cell in 1). After this introduction, a piece of literature is shortly described and thereafter evaluated.

III. RESULTS

This section contains the results of the procedure as explained in section II. The literature is given in summary in table II and further elaborated on in the rest of this section.

A. Solids

In this subsection, shape morphing strategies for solids will be discussed.

1) PRBM: In this paragraph, shape morphing applications of solids evaluated with the Pseudo Rigid Body Model [52] are discussed. This model is used to evaluate compliant members by using rigid body components and torsion springs that, when combined, have equivalent force-deflection characteristics as their compliant counterparts. While compliant mechanisms are usually modeled using continuum topology optimization

1 - Core shape morphing terms	
Shape morphing synonym	**Shape description**
Morphing	Deformed shape
Shape morphing	Deflected shape
Shape shifting	Loaded shape
Shape changing	Intermediate shape
Shape following	Initial shape
Prescribed shape	Unloaded shape
Shape programming	
Material programming	

→

2 - Focus terms	
Evaluation method	**Structure type**
Analytical	Solid
Pseudo Rigid Body Model (PRB model, PRBM)	Beam
Finite Element Method (FEM)	Shell
Inverse Finite Element Method (IFEM)	Metamaterial
	Compliant Mechanism
	Contact Aided Compliant Mechanism
	Origami
	Kirigami
	Curved Crease
	Structure

→

3 - Additional terms	
Property	**Miscellaneous**
Bistable	Synthesis
Multistable	Topology optimization
Neutrally stable	Equivalent mechanism
Force deflection	
Reconfigurable	

TABLE I: Overview of categorized search terms with increasing level of detail indicated by $1, 2, 3$.

Structure type	Method	Binary	Intermediate	Numerous
SOLID	Analytical			
	PRBM	[19]	[20]	
	FEM	[21] [18] [22] [23] [24]		
	IFEM	[25] [26] [27] [28] [29] [30] [31] [32] [33] [34]		
META MATERIAL	**Analytical**	[35] [38]	[36]	[37]
	PRBM	[39] [40]		
	FEM	[41] [43]		[42]
	IFEM			
ORIGAMI	Analytical	[44] [46]	[45] [47]	
	PRBM	[48]		
	FEM	[49]	[50] [51]	
	IFEM			

TABLE II: Literature matrix containing structure types (vertical), evaluation methods and evaluation results (horizontal).

methods coupled with the FEM, compliant flexures can also be modeled by using a PRBM.

In an effort to reduce computational costs, Schmiedeler et al. used the PRBM method to synthesize a shape morphing compliant mechanism [20] (fig. 3A) capable of approximating a shape change defined by a set of morphing curves with different shapes. A rigid body mechanism synthesis procedure was conducted by generating a chain of links that through optimization is able to approximate the morphing curves in its deformation path. The mathematical formulation used in rigid-body kinematics was then modified to include the used of compliant elements which enabled the use of PRBM's. The presented mechanism is able to follow three distinct shapes and is classified *Intermediate*.

Pucheta et al. proposed a method to design bistable compliant mechanisms by using a PRBM to model the elastic behavior of incorporated beams [19] (fig. 3B). By replacing compliant members with rigid body members that are defined by their precision position and thus using a PRBM, Pucheta et al. were able to solve for the dimensions of each beam member and use these dimensions to design for bistability. The structure is able to follow two distinct shapes and is classified *Binary*.

2) FEM: In this paragraph, shape morphing applications of solids evaluated with the Finite Element Method are discussed. Generally, this method is used to evaluate the deformed shape of an arbitrary geometry given applied loads. Uses of the FEM can be seen in many fields such as structural mechanics, automobile and aeronautics.

Vafaeesefat [21] used the FEM combined with an iterative scheme to design optimal blank geometry in sheet metal forming. The blank shape was found by minimizing the shape error between the boundary of the deformed blank and the desired shape of the deformed blank. The structure is able to follow two distinct shapes and is classified *Binary*.

Topology optimization based on boundary conditions may be used to iteratively supply input shapes for evaluation with the FEM. Lu and Kota proposed a synthesis method based on topology optimization for morphing complaint mechanisms using FEM [18](fig. 3C) that is able to morph from an initial provided geometry to a desired loaded geometry. This method is able to design for two distinct shapes and is classified *Binary*. Kirmse et al. [22] (fig. 3D) used a similar method in order to design a selective compliance shape adaptive structure that is able to warp its surface between a flat configuration and a sine shaped configuration. The structure resists unfavorable loading directions and is compliant in favorable loading directions. The structure is able to follow two distinct shapes and is classified *Binary*. Another application of this method can be seen in the design of an aircraft wing that morphs between two desired shapes by Kota et al. [23]. This method is also classified as *Binary*.

Luo et al. proposed a systematic design method for remote and wireless shape control of laminated composite structures using optimization methods [53]. The structural shape control was achieved by simultaneously seeking the best topology layouts, and thus minimizing error for desired shapes, for both the photorestrictive and elastic host layers. These desired shapes are able to be achieved with this layout by exploiting the photovoltaic effect as an actuation method. The structure is

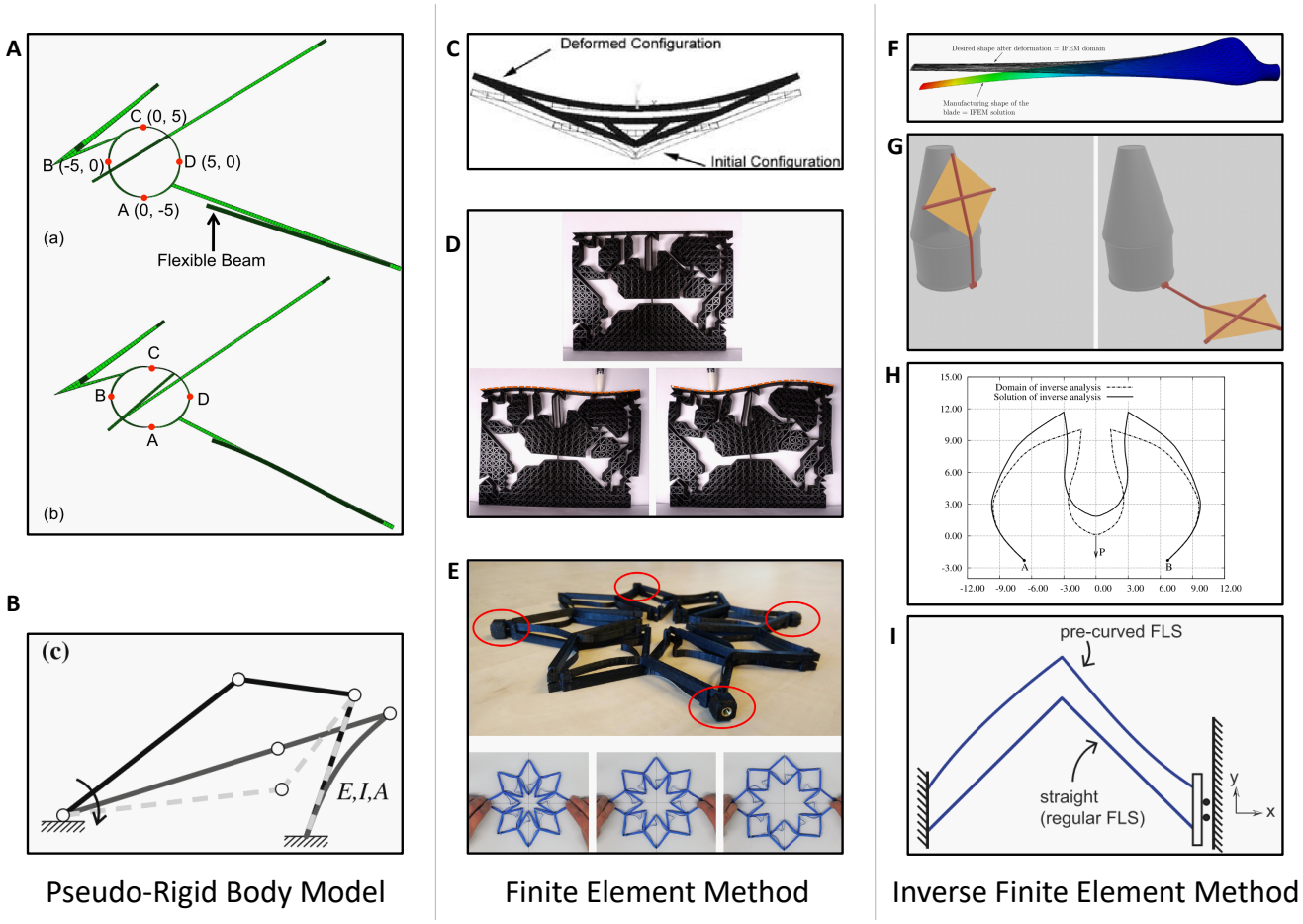

Fig. 3: Shape Morphing in Solids : **(A)** Chain of links for approximation of morphing curve by Schmiedeler et al. [20], **(B)** Bistable mechanism by Pucheta et al. [19], **(C)** Kota and Lu's method of designing for a deformed configuration using the FEM [18], **(D)** Kirmse et al.'s shape adaptive structure [22], **(E)** Compliant shape-preserving ring by Schreurs et al. [24], **(F)** Albanesi et al's method of designing for a deformed configuration using the IFEM [28], **(G)** Yellowhorse et al.'s shape fitting method [31], **(H)** Compliant gripper using IFEM by Albanesi et al. [32], **(I)** Folded leaf spring design using IFEM by Rommers et al. [34]

designed for a deformed and an initial shape, and is classified as *Binary*.

Schreurs et al. proposed a compliant shape-preserving ring for possible use in sealing mechanisms, compliant grippers or medical applications [24] (fig. 3E). Three compliant shape-preserving ring designs are presented which are able to maintain a circular outer shape in up to 99% of their full range of motion and of which the best design is able to expand in diameter by $\approx 45\%$. In order to realize these designs, a novel compliant scissor mechanism was developed through linkage system synthesis and shape optimization. The structure is able to deform continuously between an extended and a contracted shape and is classified *Binary*.

3) IFEM: In this paragraph, shape morphing applications of solids evaluated with the Inverse Finite Element Method are discussed. The Inverse Finite Element method for two- and three-dimensional isotropic elastic bodies with known loads and deformed shape was originally proposed by Mihalic and Govindjee [54], [55] and Yamada [56]. The IFEM was extended for use in three-dimensional orthotropic elastic material by Fachinotti et al. [57] and later also for elastic beams that undergo large deformations by Albanesi et al. [58].

All of the following methods are classified *Binary* since found applications of the IFEM in solids exclusively rely on finding an unloaded shape given forces and moments on the structure.

Isotropic materials have uniform properties in all directions. The IFEM for isotropic materials is used in industries such as metal forming concerning sheet metal blanks by Lu et al. [25] or automobile parts [26] by Azizi et al. [27] where the plastically deformed loaded shape is taken as a starting point in order to derive in the correct unloaded shape for the production process. Similar use can be seen in the biological field where the stress-free geometry of the abdominal aorta is determined using the in-body pressurized geometry.

Orthotropic materials have directionality dependent proper-

ties and are of particular interest in fields like turbine blade design or deep drawing of orthotropic metals. Albanesi et al., in an attempt to reduce weight and cost, used this method to design the optimal geometry of laminated wind turbine blades [28] (fig. 3F). By designing the loaded shape of these laminated wind turbine blades and using the orthotropic IFEM formulation, Albanesi determined the initial shape such that it deformed correctly under a specified load. This inverse method is also used in the determination of the optimal blank shape from the desired shape in deep drawing of steel. by Kim et al. [29] and Germain et al. [30].

Besides acquiring the initial unloaded shape from a deformed loaded shape, the IFEM also allows to solve for the loads that allow morphing between these two states. Yellowhorse et al. proposed a method for deriving the loads needed to approximate a desired, relaxed state of a beam given the stressed state [31] (fig. 3G). A given example of an application of such a structure is a folded solar panel to a rocket geometry. The proposed method was observed to function with multiple fitting points or stressed states.

The inverse elastic beam model by Albanesi et al. [58] allows for lower computational costs than previously discussed more general methods due to simplification by using beam elements. Albanesi demonstrated this method in the design of structures where a beam simplification can be made such as a compliant gripper or a car wiper blade [32] (fig. 3H).

In an effort to increase computational efficiency over conventional forward iterative methods of design, Bertail et al. used the IFEM method for beams in acquiring the initial unloaded shape of an Kirchoff rod [33]. A Kirchoff rod is a thin elastic rod which can be useful in the modelling of beam-like structures such as DNA, hair or climbing plants.

Another use of the IFEM for beams is proposed by Rommers et al. in the design of a folded leaf spring flexure [34] (fig. 3I). For a linear guide, a high support stiffness is desirable in both non-actuated and actuated state of the structure. Rommers et al. used the IFEM to generate the unloaded initial shape of the folded leaf spring from the optimal actuated shape, and used this alongside a folded leaf spring with an optimal shape in the unloaded configuration. This allowed for higher support stiffness over the displacement range than a combination of two non-curved regular folded leaf springs.

B. Meta Materials

In this subsection, shape morphing strategies for metamaterials will be discussed.

1) ANALYTICAL: In this paragraph, shape morphing applications of metamaterials evaluated with analytical methods are discussed.

Jiang et al. proposed a shape morphing metamaterial capable of morphing into three-dimensional shapes [35] (fig. 4A). Jiang was able to design cut patterns such that the initial planar material is able to deploy continuously to a given surface as well as a non-flat initial surface to a planar cut pattern. The design is derived by using an analytical model combined with an optimizer to create the correct pattern to map between the two shapes. The structure is able to follow two distinct shapes and is classified *Binary*.

A multistable metamaterial was proposed by Che et al. [36] (fig. 4B). The material uses snap-through instability of flexible members order to retain its shape in multiple positions after deformation. The deformation sequence in which each segment snaps to another state upon induced strain can be tuned by varying the beam thickness for each elastic segment. By assuming small rotations, Che was able to derive an analytical model which was able to yield comparable deformation estimation results to Finite Element Analysis. The structure is able to follow five distinct shapes and is classified *Intermediate*.

A reconfigureable structure inspired by polyhedron linkages as proposed by Liu et al. [37] (fig. 4C) allows for tunable properties like Poisson's Ratio or stiffness by the use of kinematic bifurcations. A kinematic bifurcation arises when two different paths of the same structure intersect. The *Wohlhart-polyhedron* as proposed by Liu achieves its motion through rigid links with folds connected to a square center body. Liu et al. used an analytical model for simulating the Poisson's Ratio of a tessellation of modules. The structure is able to be configured in more than 10 distinct designed shapes and is classified *Numerous*.

Attard et al. proposed a similar auxetic structure consisting, of cuboidal rotating rigid units connected together at their edges [38]. An analytical model was derived for the Poisson's Ratio and Young's Modulus of the structure. It was shown that the structure exhibits negative values for all the six on-axis Poisson's ratios when loaded on-axis. The structure has a single degree of freedom and can either be closed or (partially) open. Therefore two distinct shapes are assumed and this structure is classified *Binary*.

2) PRBM: In this paragraph, shape morphing applications of metamaterials evaluated with the Pseudo Rigid Body Model are discussed. A Mmetamaterial containing at least one flexible part that can be modeled as a beam in it's unit cell can benefit from employing the PRBM for improvements in computational costs. Although the usage of PRBM's in Meta Materials is novel, some uses can be found.

Broeren et al. proposed the use of a PRBM for the analysis of a spatial mechanical Meta Material [39] (fig. 4D) The use of this model enabled Broeren to determine the post-buckling behavior of the Meta Material without the need to consider the whole elastic structure and thus avoid the use of FEM. The analysis was conducted on a porous cylindrical structure, consisting of rigid squares at their corners. Two PRBM's were presented. The first one, a simplified version of the Meta Material with a single variable, was able to capture the main features of the structure in the post-buckling regime but was still coarse due to the inability to include boundary conditions introduced by the clamping of the structure. The second one, with one variable per non-boundary layer of the structure, was able to capture the experimental boundary conditions and math the observed Poisson's Ratio and force-displacement behavior

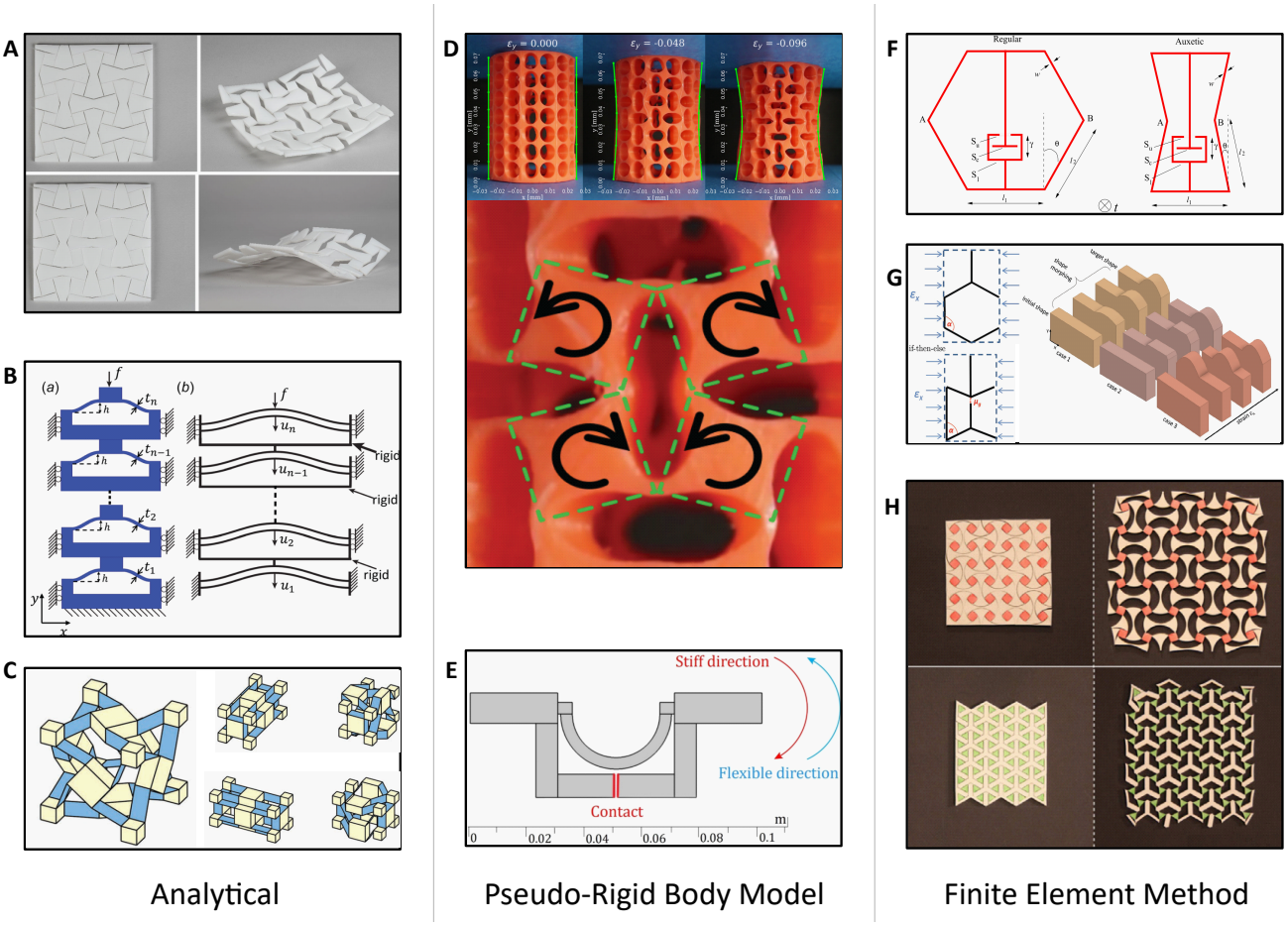

Fig. 4: Shape Morphing in Meta Materials : **(A)** shape morphing Meta Material by Jiang et al. [35], **(B)** Multistable Meta Material by Che et al. [36], **(C)** Reconfigureable structure by Liu et al. [37], **(D)** Spatial mechanical Metamaterial by Broeren et al. [39], **(E)** Cellular Contact Aided Compliant Mechanism by Hargrove et al. [40], **(F)** Progammable unit-cell by Mehta et al. [41], **(G)** Morphing Metamaterial by Wenz et al. [42],**(H)** A bistable Meta Material by Rafsanjani et al. [43]

of the structure more accurately. The proposed method is able to describe an initial and a deformed shape and is classified *Binary*.

Another use of the PRBM was proposed by Hargrove et al. [40] (fig. 4E), who designed a *Cellular Contact Aided Compliant Mechanism* that exhibits nonlinear stiffness behavior. The mechanism utilizes a semicircular compliant beam to enable flexibility in one direction and stiffness in the other direction by making internal contact. The mechanism exhibits nonlinear stiffness behavior between two distinctly shaped topological configurations and is classified *Binary*.

3) FEM: In this paragraph, shape morphing applications of metamaterials evaluated with the Finite Element Method are discussed.

Based on a regular honeycomb unit-cell design, Mehta et al. as well as Wenz et al. proposed a new type of programmable unit-cell that introduces a cantilever beam in the design [41] [42] (fig. 4F, fig. 4G). The addition of this cantilever beam in Wenz's design introduces an extra parameter, gap length μ_g, which can be used to tune the non-linear stiffness behavior in the unit-cell upon internal contact analogous to processing functions used in informatics. Three types of strain-induced shape morphing cases are presented which exhibit unique morphing behavior. While Mehta et al.'s proposed mechanism is classified as *Binary* due to it's two topological configurations, Wenz et al's proposed structure consists of many of such unit cells which are theoretically able to follow near infinitely many distinct designed shapes. Wenz et al's presented method and structure are able to follow more than ten shapes and are therefore classified as *Numerous*.

By exploiting bi- or multistability, Meta Materials can be able to retain their shape after deformations. A bistable Meta Material inspired by ancient geometric motifs was proposed by Rafsanjani et al. [43] (fig. 4H). This planar Meta Material consists of a network of rotating units connected with compliant hinges, which through snap-through instabilities allow for bistability and auxetic behavior. Due to the bistable behavior of the structure it is classified as *Binary*.

C. Origami

In this subsection, shape morphing strategies for origami structures will be discussed.

1) ANALYTICAL: In this paragraph, shape morphing applications of Origami structures evaluated with analytical methods are discussed.

The kinematics of Origami structures can be modelled in a variety of ways including direct geometric formulation, equivalent mechanisms, such as a spherical model [60] [61] or Denavit-Hartenberg (D-H) parameter setup [62], or reduced-order methods which allow for describing the main behavior of complex models once simplification hypotheses such as symmetry or other conditions are fulfilled.

A direct geometric formulation can be used when the Origami structure is assumed rigidly foldable, in other words all motion happens due to deflection at the crease lines. Lee et al. used a direct geometric approach in the modeling of a deformable wheel for a robot [44], capable of varying it's radius by pushing the sides of the wheel. By constructing a kinematic model of this structure, the deformation and shape of the structure could be accurately predicted. While the outer radius of the wheel could be derived analytically, numerical tools were used in solving the remaining equations due to occurring nonlinearities. The structure is able to deform continuously between an extended and a contracted shape and is classified *Binary*.

Li et al. used a kinematic approach in the proposal of a multifunctional adaptive fluidic origami concept [59] (fig. 5C). By taking advantage of the relation between folding motion and the enclosed internal fluid volume, the structure is able to achieve autonomous shape morphing and stiffness tailoring. The analytical kinematic model was developed based on a unit cell of fluidic origami with reinforced periodic boundary conditions. The structure is able to deform between an extended and a contracted shape and is classified *Binary*.

Enabling multiple distinct shapes in a structure may also be achieved by exploiting bi- or multistability. Jianguo et al. proposed a bistable cylindrical Origami structure based on a Kresling pattern [45]. The structure was studied using an analytical model, which concluded that for a certain ratio of geometric parameters bistability was present. The bistability was found to be caused by two minima of strain energy present in the deformation path. The presented structure consists of four segments and therefore five distinct configurations and is classified *Intermediate*.

Fonseca et al. proposed an Origami wheel actuated by shape memory alloy actuators [46]. Shape memory alloys can be deformed when below a certain temperature, but return to their pre-deformed shape when heated. When a SMA actuator is deployed on the circumference of the wheel, shape change can be induced by heating and cooling the SMA. Due to symmetry, the model could be simplified to a 1-DOF system. A reduced-order model was used to describe the origami dynamics. The structure is able to deform between an extended and a contracted shape and is classified *Binary*.

Another strategy to achieve distinct multiple shapes is structural reconfigurability. Overvelde et al. proposed a design strategy for reconfigurable architected materials, and explored this design space by considering structures based on tessellations of polyhedra [47] (fig. 5B). With this strategy, three-dimensional reconfigurable materials comprising of a periodic assembly of rigid plates and elastic hinges were explored and different deformation modes and internal arrangements were identified. The structures presented have a range of two to four unique deformation modes and are classified *Intermediate*.

Choi et al. proposed a design method for compact reconfigurable kirigami structures by introducing an intermediate shape through which shape morphing between a compact configuration and an open deployed shape and can be realized [49] (fig. 5A). By recognition and generalization of the analytical geometric constraints that describe said kirigami structures, Choi et al. were able to use an optimization scheme that is able to approximate an optimal configuration that matches the target shapes and satisfies the reconfigurability conditions. The structure presented is able to morph between two distinct provided shapes, and an intermediate shape and is classified *Binary*.

2) PRBM: In this paragraph, shape morphing applications of Origami structures evaluated with the Pseudo Rigid Body Model are discussed.

Rommers et al. used the PRBM to model the bending behavior of the bottom facets of a Single Vertex Compliant Facet Origami Mechanism [48] (fig. 5D). SV-COFOM's are a special type of origami structure in which the compliance of the facets is used to incorporate spring behavior. The usage of the PRBM allows for a simpler, yet accurate model that is able to compute the moment curve of the structures as a function of a given angle. The structure is able to deform between an extended and a contracted shape and is classified *Binary*.

3) FEM: In this paragraph, shape morphing applications of Origami structures evaluated with the Finite Element Method are discussed. While the FEM can be used for simulating the stretching, shearing and bending behavior of Origami structures accurately [63] [64], it can prove challenging due to high computational costs or not fitting for certain geometries depending on the discretization technique. A more general applicable method to different folding patterns with a sufficient accuracy to capture the elastic behavior at a lower computational cost, is the bar-hinge model. The bar-hinge model was originally proposed by Schenk et al. [65] and Wei et al. [66] and later expanded upon to include in-plane deformations by Filipov et al. [67]. Woodruff et al. later expanded further on this work by incorporating curved-crease Origami [68] [69] in the bar-hinge model.

Curved crease Origami can be modeled and deformed in such a way to allow for neutral stability, which means that the structure is able to maintain a constant elastic potential energy during deformation. This enables equilibrium over a significant portion of its deformation range. This neutrally stable behavior is exceptional, since deforming structures usually build up elastic potential energy which results in

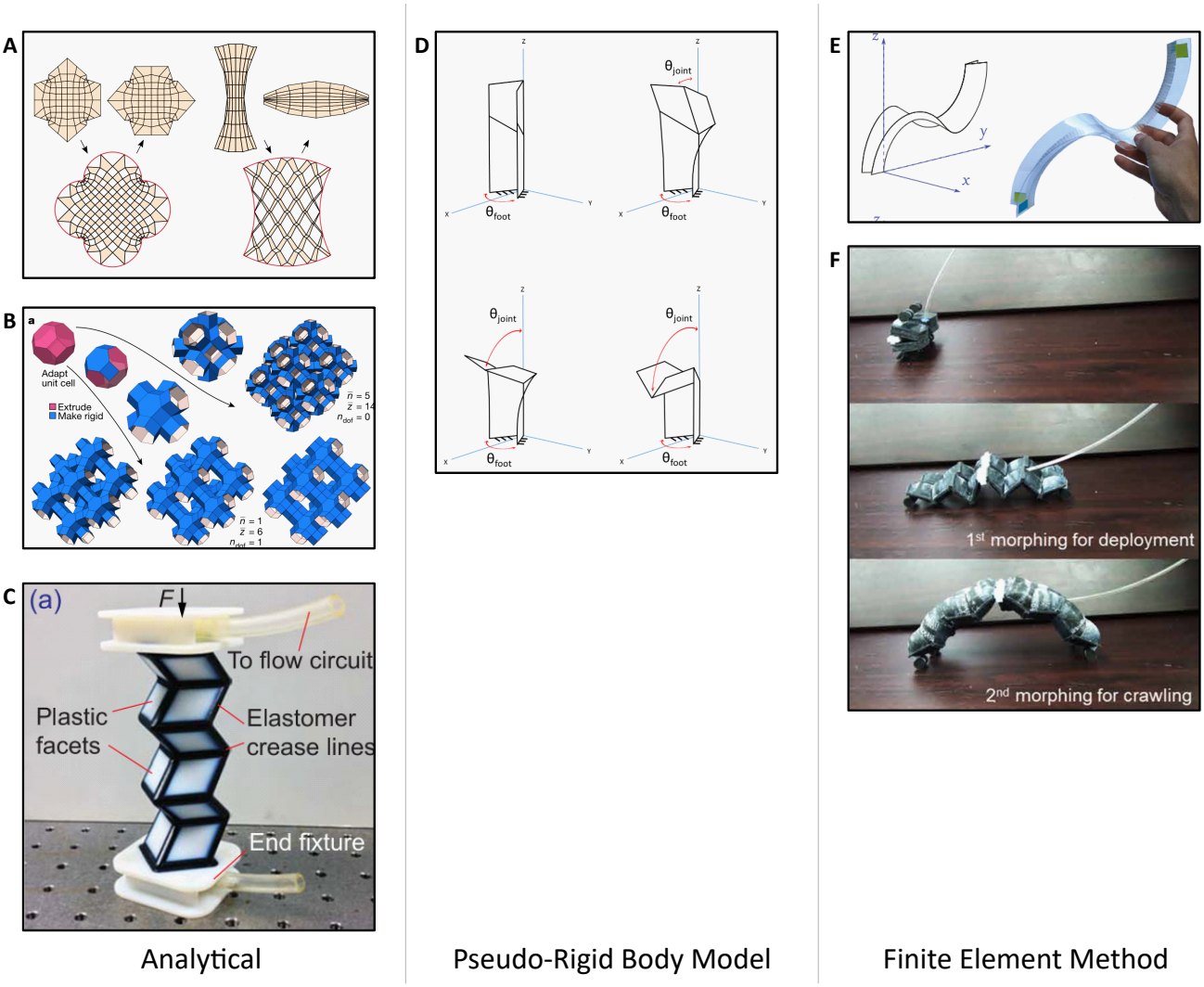

Fig. 5: Shape Morphing in Origami Structures : **(A)** Compact reconfigurable kirigami structures by Choi et al. [49], **(B)** Reconfigurable architected materials by Overvelde et al. [47], **(C)** Multifunctional adaptive fluidic origami concept by Li et al. [59], **(D)** Single Vertex Compliant Facet Origami Mechanism by Rommers et al. [48], **(E)** Neutrally stable curved crease origami structure by Kok et al. [50], **(F)** Bioinspired dual-morphing stretchable origami by Kim et al. [51]

an opposing force or moment. Kok et al. proposed such a structure [50] (fig. 5E), which consists of two flat arched-shaped compliant sheets which are stacked and connected along one side which functions as a hinge. The structure has three stable positions, two of which are the fabricated and inverted fabricated positions. The third position exists within an energetic equilibrium and can be varied over a significant range of motion, between the fabricated and the inversed fabricated position. The energetic path during the transition of this structure can be tuned by manipulating the crease curvature as well as the local width. The structure has three stable positions and is classified *Intermediate*.

A bio-inspired dual-morphing stretchable origami was proposed by Kim et al. [51] (fig. 5F). A dual-morphing structure is capable of unfolding from its initial state and stretching its skin to enable shape morphing. In the study, the design of a pellcan eel inspired structure is explored that embodies quasi-sequential behavior of origami by unfolding and stretching its skin in response to a change in fluid pressure. A Finite Element Analysis study was conducted to study the angle and transition pressure between modules of the structure. The structure has three designed positions and is classified *Intermediate*.

IV. DISCUSSION

Designing strategies for shape morphing structures with multiple distinct shapes during their working conditions still remains a challenge due to physical limitations, added complexity or the absence of knowledge. Research into structures that morph into multiple distinct shapes still remains relatively scarce. As can be seen in fig. 1, for some categories no literature was found. This absence can be attributed due to the

novelty of the evaluation method combined with this structure type, or the usability thereof.

As can be concluded from table II, solids currently lack the functional complexity that is required for complex shape morphing. This structure type does however have a solid basis for binary shape morphing due to its ample studies into applications in FEM and IFEM. The lack of analytical methods being used in solids can be explained by the complexity of describing the morphing behavior of complicated shapes. Unlike meta materials and origami structures, where morphing behaviour can often be simplified using simplified models, such simplifications generally do not come into play when describing the shape morphing behavior of solids. When the shape of a solid is important, it is usually too complex to describe analytically.

The use of metamaterials for shape morphing purposes might prove to be successful due to the possible complex behavior made possible by use of varying unit-cells, bi- or multistability, or cut and fold patterns in a structure. The shape morphing behavior of metamaterial unit-cells is analytically generally well understood. This knowledge enables designers to extrapolate these characteristics to describe an array of these sub-structures. The use of the PRBM in meta materials can be beneficial to simplify a model and thus decrease computational cost, but remains relatively unused. Computational cost gains of deploying PRBM over FEM are generally negligible when considering the general description of a single cell, but could provide to be useful when an multiple unit-cells get simulated in parallel for varying properties inside a structure. The IFEM is a novel technique, and due to this it has not been applied in the field of meta material shape morphing, but might prove useful if deformations are involved.

Origami structures might also prove to be successful for shape morphing applications due to their enhanced mobility introduced by cuts and folds. Analytical methods are readily used to describe the kinematics of these structures. The use of IFEM in origami structures has not been explored yet and might prove to be limited in use due to the mostly rigid facets present in origami structures. If these facets are however not assumed rigid and deformations can be present, IFEM might prove useful in future work.

The used categorisation in in fig. 1 provides a clear distinction between the different structure types commonly found in shape morphing, however there is overlap possible between these types. In this case, the best fitting structure type is chosen based on given literature. If an overlap is present, the assessment of structure type could also be chosen in a different way. This particular assessment of structure type proves a limitation to the used categorisation method. In future work, other structure types or evaluation methods may arise that present yet unexplored functionalities. These structure types or evaluation methods could be introduced or used as a replacement in fig. 1. Another limiting factor in this study is the ambiguity in describing certain phenomena. Different pieces of literature can for example describe the shape morphing mechanism using different terms. An effort is made in table I by including synonyms that cover the same topic. Certain descriptions may have not be included due to their description being too different from the commonly used terms in this field.

In future literature reviews on shape morphing phenomena, the scope of evaluation methods could be increased by including literature based on other structure types or evaluation methods than given in fig. 1. While many studies on Origami Structures use methods described in this literature review to validate their results, a large amount of promising shape morphing papers have been excluded from this literature review due to their use of experimental design methods [70], thereby limiting the scope of this literature review.

With the predominant use of FEM and IFEM in shape morphing studies for solids, more effort could be put into allowing introduction of intermediate distinct shapes. Possible means to aid in this challenge could be by combining aforementioned methods or using iterative schemes to derive an approximation of all desired shapes. However, limitations in approximating said shapes may still arise due to limitations in structure flexibility or limitations in structure capabilities. If these limitations arise, other methods of enabling complex shape morphing behaviour may be explored by for example introducing additional external stimuli or actuators.

Future relevant work in the field of shape morphing capabilities may be research into the approximation of multiple shapes during the deformation of a structure, combined with a desirable force-deflection characteristic of said structure. Due to the influence of the shape of a structure on its exerted force and vice-versa, this might prove to be a challenge for future scientists and engineers.

V. CONCLUSION

A literature study is presented on shape morphing methods and strategies in order to provide an overview, evaluation and interpretation on the current advancements in the field. Literature is analysed based on relevance criteria. It is then classified based on the underlying evaluation methods such as FEM, IFEM, PRBM and analytical methods, as well as on structure types such as solids, Meta Materials and Origami structures. Shape morphing methods and strategies in the literature in these categories are then evaluated based on how many distinct shapes they are able to follow during their deformation path. The results of this study show that while a lot of research has been conducted on structures that are able to morph in shape between two user provided shapes, the amount of research conducted on shape morphing strategies and methods that go beyond this *Binary* classification into *Intermediate* or even *Numerous* is still relatively small. It is concluded the underresearch is to be attributed to bottlenecks that arise due to the added complexity and increased computational cost as well as material limitations and the novelty of the research field.

REFERENCES

[1] R. M. Fowler, L. L. Howell, and S. P. Magleby, "Compliant space mechanisms: A new frontier for compliant mechanisms," *Mechanical Sciences*, vol. 2, no. 2, pp. 205–215, 2011.

[2] L. L. Howell, "Compliant Mechanisms," in *21st Century Kinematics*. Springer London, 2013, pp. 189–216.

[3] J. A. Gallego and J. Herder, "Synthesis methods in compliant mechanisms: An overview," Tech. Rep. PARTS A AND B, 2009.

[4] B. A. Salamon and A. Midha, "An Introduction to Mechanical Advantage in Compliant Mechanisms," *Journal of Mechanical Design*, vol. 120, no. 002, p. 311, 1998.

[5] E. Barchiesi, M. Spagnuolo, and L. Placidi, "Mechanical metamaterials: a state of the art," *Mathematics and Mechanics of Solids*, vol. 24, no. 1, pp. 212–234, 1 2019.

[6] J. U. Surjadi, L. Gao, H. Du, X. Li, X. Xiong, N. X. Fang, and Y. Lu, "Mechanical Metamaterials and Their Engineering Applications," 3 2019.

[7] N. Turner, B. Goodwine, and M. Sen, "A review of origami applications in mechanical engineering," pp. 2345–2362, 8 2016.

[8] L. Yin and G. K. Ananthasuresh, "Design of distributed compliant mechanisms," *Mechanics Based Design of Structures and Machines*, vol. 31, no. 2, pp. 151–179, 2003.

[9] X. Ren, R. Das, P. Tran, T. D. Ngo, and Y. M. Xie, "Auxetic metamaterials and structures: A review," 1 2018.

[10] C. G. Gou and Yang L, "Research on Multistable Compliant Mechanisms: The State of the Art," Tech. Rep., 2010.

[11] Z. Wang, L. Jing, K. Yao, Y. Yang, B. Zheng, C. M. Soukoulis, H. Chen, and Y. Liu, "Origami-Based Reconfigurable Metamaterials for Tunable Chirality," *Advanced Materials*, vol. 29, no. 27, 7 2017.

[12] V. Charpentier, P. Hannequart, S. Adriaenssens, O. Baverel, E. Viglino, and S. Eisenman, "Kinematic amplification strategies in plants and engineering," 5 2017.

[13] Y. Li, Y. Zhao, Y. Chi, Y. Hong, and J. Yin, "Shape-morphing materials and structures for energy-efficient building envelopes," 12 2021.

[14] S. Vasista, O. Mierheim, and M. Kintscher, "Morphing Structures, Applications of," in *Encyclopedia of Continuum Mechanics*. Springer Berlin Heidelberg, 2019, pp. 1–13.

[15] S. Daynes and P. M. Weaver, "Review of shape-morphing automobile structures: Concepts and outlook," Tech. Rep. 11, 2013.

[16] F. Fiorito, M. Sauchelli, D. Arroyo, M. Pesenti, M. Imperadori, G. Masera, and G. Ranzi, "Shape morphing solar shadings: A review," pp. 863–884, 3 2016.

[17] A. Midha, T. W. Norton, and L. L. Howell, "On the nomenclature, classification, and abstractions of compliant mechanisms," Tech. Rep. 1, 1994. [Online]. Available: http://www.asme.org/about-asme/terms-of-use

[18] K. J. Lu and S. Kota, "Design of compliant mechanisms for morphing structural shapes," *Journal of Intelligent Material Systems and Structures*, vol. 14, no. 6, pp. 379–391, 2003.

[19] M. A. Pucheta and A. Cardona, "Design of bistable compliant mechanisms using precision-position and rigid-body replacement methods," *Mechanism and Machine Theory*, vol. 45, no. 2, pp. 304–326, 2010. [Online]. Available: http://dx.doi.org/10.1016/j.mechmachtheory.2009.09.009

[20] J. P. Schmiedeler and A. P. Murray, "Kinematic Synthesis of Planar, Shape-Changing Compliant Mechanisms," pp. 1–12, 2012.

[21] A. Vafaeesefat, "Finite element simulation for blank shape optimization in sheet metal forming," *Materials and Manufacturing Processes*, vol. 26, no. 1, pp. 93–98, 2011.

[22] S. Kirmse, L. F. Campanile, and A. Hasse, "Synthesis of compliant mechanisms with selective compliance – An advanced procedure," *Mechanism and Machine Theory*, vol. 157, 3 2021.

[23] S. Kota, J. A. Hetrick, R. Osborn, D. Paul, E. Pendleton, P. Flick, and C. Tilmann, "Design and application of compliant mechanisms for morphing aircraft structures," Tech. Rep., 2003.

[24] K. W. Schreurs, G. Radaelli, and F. Alijani, "The design of a compliant shape-preserving ring," *Mechanism and Machine Theory*, vol. 151, 2020.

[25] R. Azizi and A. Assempour, "Applications of linear inverse finite element method in prediction of the optimum blank in sheet metal forming," *Materials and Design*, vol. 29, no. 10, pp. 1965–1972, 2008.

[26] C. H. Lee and H. Huh, "Blank design and strain prediction of automobile stamping parts by an inverse finite element approach," *Journal of Materials Processing Technology*, vol. 63, no. 1-3, pp. 645–650, 1997.

[27] J. Lu, X. Zhou, and M. L. Raghavan, "Inverse elastostatic stress analysis in pre-deformed biological structures: Demonstration using abdominal aortic aneurysms," *Journal of Biomechanics*, vol. 40, no. 3, pp. 693–696, 2007.

[28] A. Albanesi, F. Bre, V. Fachinotti, and C. Gebhardt, "Simultaneous ply-order, ply-number and ply-drop optimization of laminate wind turbine blades using the inverse finite element method," *Composite Structures*, vol. 184, pp. 894–903, 1 2018.

[29] S. H. Kim, S. H. Kim, and H. Huh, "Finite element inverse analysis for the design of intermediate dies in multi-stage deep-drawing processes with large aspect ratio," *Journal of Materials Processing Technology*, vol. 113, no. 1-3, pp. 779–785, 2001.

[30] S. Germain and P. Steinmann, "Towards inverse form finding methods for a deep drawing steel DC04," *Key Engineering Materials*, vol. 504-506, pp. 619–624, 2012.

[31] A. Yellowhorse, J. Rommers, A. Amoozandeh, and J. L. Herder, "Methods for shape fitting in morphing compliant mechanisms," Tech. Rep., 2021.

[32] A. E. Albanesi, V. D. Fachinotti, and A. Cardona, "Design of Compliant Mechanisms that Exactly Fit a Desired Shape," *Mecánica Computacional*, vol. 38, no. 38, pp. 3191–3205, 2009.

[33] F. Bertails-Descoubes, A. Derouet-Jourdan, V. Romero, and A. Lazarus, "Inverse design of an isotropic suspended Kirchhoff rod: Theoretical and numerical results on the uniqueness of the natural shape," *Proceedings of the Royal Society A: Mathematical, Physical and Engineering Sciences*, vol. 474, no. 2212, 2018.

[34] J. Rommers and J. L. Herder, "Design of a Folded Leaf Spring with high support stiffness at large displacements using the Inverse Finite Element Method," in *Mechanisms and Machine Science*, vol. 73. Springer Science and Business Media B.V., 2019, pp. 2109–2118.

[35] C. Jiang, F. Rist, H. Wang, J. Wallner, and H. Pottmann, "Shape-morphing mechanical metamaterials," *CAD Computer Aided Design*, vol. 143, 2 2022.

[36] K. Che, C. Yuan, J. Wu, H. J. Qi, and J. Meaud, "Three-dimensional-printed multistable mechanical metamaterials with a deterministic deformation sequence," *Journal of Applied Mechanics, Transactions ASME*, vol. 84, no. 1, 1 2017.

[37] W. Liu, H. Jiang, and Y. Chen, "3D Programmable Metamaterials Based on Reconfigurable Mechanism Modules," *Advanced Functional Materials*, vol. 32, no. 9, 2 2022.

[38] D. Attard and J. N. Grima, "A three-dimensional rotating rigid units network exhibiting negative Poisson's ratios," *Physica Status Solidi (B) Basic Research*, vol. 249, no. 7, pp. 1330–1338, 2012.

[39] F. G. Broeren, V. van der Wijk, and J. L. Herder, "Spatial pseudo-rigid body model for the analysis of a tubular mechanical metamaterial," *Mathematics and Mechanics of Solids*, vol. 25, no. 2, pp. 305–316, 2020.

[40] B. Hargrove, A. Nastevska, M. Frecker, and J. Jovanova, "Pseudo Rigid Body Model for Nonlinear Folding Contact-Aided Compliant Mechanism," *SSRN Electronic Journal*, no. 1, 2022.

[41] V. Mehta, M. Frecker, and G. Lesieutre, "Contact-aided compliant mechanisms for morphing aircraft skin," in *Modeling, Signal Processing, and Control for Smart Structures 2008*, vol. 6926. SPIE, 3 2008, p. 69260C.

[42] F. Wenz, I. Schmidt, A. Leichner, T. Lichti, S. Baumann, H. Andrae, and C. Eberl, "Designing Shape Morphing Behavior through Local Programming of Mechanical Metamaterials," *Advanced Materials*, vol. 33, no. 37, 9 2021.

[43] A. Rafsanjani and D. Pasini, "Bistable auxetic mechanical metamaterials inspired by ancient geometric motifs," *Extreme Mechanics Letters*, vol. 9, pp. 291–296, 12 2016.

[44] D. Y. Lee, J. S. Kim, S. R. Kim, J. S. Koh, and K. J. Cho, "The deformable wheel robot using magic-ball origami structure," in *Proceedings of the ASME Design Engineering Technical Conference*, vol. 6 B, 2013. [Online]. Available: http://www.asme.org/about-asme/terms-of-use

[45] C. Jianguo, D. Xiaowei, Z. Ya, F. Jian, and T. Yongming, "Bistable behavior of the cylindrical origami structure with Kresling pattern," *Journal of Mechanical Design, Transactions of the ASME*, vol. 137, no. 6, p. 1DUMMMY, 6 2015.

[46] L. M. Fonseca, G. V. Rodrigues, M. A. Savi, and A. Paiva, "Nonlinear dynamics of an origami wheel with shape memory alloy actuators," *Chaos, Solitons and Fractals*, vol. 122, pp. 245–261, 2019. [Online]. Available: https://doi.org/10.1016/j.chaos.2019.03.033

[47] J. T. Overvelde, J. C. Weaver, C. Hoberman, and K. Bertoldi, "Rational design of reconfigurable prismatic architected materials," *Nature*, vol. 541, no. 7637, pp. 347–352, 1 2017.
[48] J. Rommers, G. Radaelli, and J. Herder, "A Pseudo Rigid Body model of a Single Vertex Compliant-Facet Origami Mechanism (SV-COFOM)," *Proceedings of the ASME Design Engineering Technical Conference*, vol. 5B-2016, pp. 1–10, 2016.
[49] G. P. Choi, L. H. Dudte, and L. Mahadevan, "Compact reconfigurable kirigami," *Physical Review Research*, vol. 3, no. 4, pp. 1–16, 2021.
[50] S. Kok, G. Radaelli, A. Amoozandeh Nobaveh, and J. Herder, "Neutrally stable transition of a curved-crease planar shell structure," *Extreme Mechanics Letters*, vol. 49, 11 2021.
[51] W. Kim, J. Byun, J. K. Kim, W. Y. Choi, K. Jakobsen, J. Jakobsen, D. Y. Lee, and K. J. Cho, "Bioinspired dual-morphing stretchable origami," *Science Robotics*, vol. 4, no. 36, pp. 1–11, 2019.
[52] L. L. Howell and A. Midha, "A method for the design of compliant mechanisms with small-length flexural pivots," *Journal of Mechanical Design, Transactions of the ASME*, vol. 116, no. 1, pp. 280–290, 1994.
[53] Z. Luo, Q. Luo, L. Tong, W. Gao, and C. Song, "Shape morphing of laminated composite structures with photostrictive actuators via topology optimization," *Composite Structures*, vol. 93, no. 2, pp. 406–418, 2011. [Online]. Available: http://dx.doi.org/10.1016/j.compstruct.2010.09.001
[54] S. Govindjee and P. A. Mihalic, "Computational methods for inverse finite elastostatics," *Computer Methods in Applied Mechanics and Engineering*, vol. 136, no. 1-2, pp. 47–57, 1996.
[55] ——, "Computational methods for inverse deformations in quasi-incompressible finite elasticity," *International Journal for Numerical Methods in Engineering*, vol. 43, no. 5, pp. 821–838, 1998.
[56] T. Yamada, "Finite element procedure of initial shape determination for hyperelasticity," *Structural Engineering and Mechanics*, vol. 6, no. 2, pp. 173–183, 1998.
[57] V. D. Fachinotti, A. Cardona, and P. Jetteur, "Finite element modelling of inverse design problems in large deformations anisotropic hyperelasticity," *International Journal for Numerical Methods in Engineering*, vol. 74, no. 6, pp. 894–910, 5 2008.
[58] A. E. Albanesi, V. D. Fachinotti, and A. Cardona, "Inverse Analysis of Large-Displacement Beams," *Mecánica Computacional*, vol. 27, no. December, pp. 1049–1061, 2008. [Online]. Available: http://www.cimec.org.ar//www.amcaonline.org.ar
[59] S. Li and K. W. Wang, "Fluidic origami: A plant-inspired adaptive structure with shape morphing and stiffness tuning," *Smart Materials and Structures*, vol. 24, no. 10, 9 2015.
[60] L. A. Bowen, C. L. Grames, S. P. Magleby, L. L. Howell, and R. J. Lang, "A classification of action origami as systems of spherical mechanisms," *Journal of Mechanical Design, Transactions of the ASME*, vol. 135, no. 11, pp. 1–7, 2013.
[61] R. L. P. Barreto, F. V. Morlin, M. B. de Souza, A. P. Carboni, and D. Martins, "Multiloop origami inspired spherical mechanisms," *Mechanism and Machine Theory*, vol. 155, 2021.
[62] J. Denavit and R. S. Hartenberg, "A Kinematic Notation for Lower-Pair Mechanisms Based on Matrices," pp. 215–221, 1955.
[63] M. Schenk and S. D. Guest, "On zero stiffness," pp. 1701–1714, 2014.
[64] C. Lv, D. Krishnaraju, G. Konjevod, H. Yu, and H. Jiang, "Origami based mechanical metamaterials," *Scientific Reports*, vol. 4, 2014.
[65] M. Schenk, "Folded Shell Structures," no. August, p. 149, 2011. [Online]. Available: http://www.markschenk.com/research/files/PhD thesis - Mark Schenk.pdf
[66] Z. Y. Wei, Z. V. Guo, L. Dudte, H. Y. Liang, and L. Mahadevan, "Geometric mechanics of periodic pleated origami," *Physical Review Letters*, vol. 110, no. 21, pp. 1–5, 2013.
[67] E. T. Filipov, K. Liu, T. Tachi, M. Schenk, and G. H. Paulino, "Bar and hinge models for scalable analysis of origami," *International Journal of Solids and Structures*, vol. 124, pp. 26–45, 2017.
[68] S. R. Woodruff and E. T. Filipov, "A bar and hinge model formulation for structural analysis of curved-crease origami," *International Journal of Solids and Structures*, vol. 204-205, pp. 114–127, 2020. [Online]. Available: https://doi.org/10.1016/j.ijsolstr.2020.08.010
[69] ——, "Bending and twisting with a pinch: Shape morphing of creased sheets," *Extreme Mechanics Letters*, vol. 52, 4 2022.
[70] A. Chortos, J. Mao, J. Mueller, E. Hajiesmaili, J. A. Lewis, and D. R. Clarke, "Printing Reconfigurable Bundles of Dielectric Elastomer Fibers," *Advanced Functional Materials*, vol. 31, no. 22, pp. 1–10, 2021.

Multi Shape-Morphing: A Design Method for a Parametric Beam Based Exoskeleton

Jasper Pels, Giuseppe Radaelli
Department of Precision and Microsystems Engineering, Delft University of Technology

***Abstract*—The bending stiffness of a structure is highly dependent on its shape, and this relation can be utilized to allow for a structure to morph into different shapes during deformation. This paper focuses on shape-morphing into multiple shapes (Multi Shape-Morphing), and presents a design method for a parametric structure consisting of beams, that is able to approximate a set of objective shapes during deformation by exploiting its geometry. Several designs are generated with this design method and experimental validation has been performed on several physical models verify the multi shape-morphing performance. A sensitivity analysis has been conducted on relevant design variables of generated designs to identify their relative importance concerning the structure's multi shape-morphing performance. To demonstrate the feasibility of the proposed design method for use with exoskeletons, a human-scaled prototype has been designed, and validated.**

I. Introduction

The demand for more efficient components in industries such as biomedical [1], high-tech [2] and space [3] is rapidly increasing. To meet this demand, engineers are constantly seeking novel techniques to improve the precision, reliability, and capabilities of their designs. A promising and developing research field that seeks to aid in these challenges is the development of compliant mechanisms [4], [5], which gain at least part of their mobility through deflection of flexible members. Research into compliant mechanisms is conducted in many areas such as synthesis methods [6], designing for function such as required deflection [7] or load-path characteristics [8], hinge design [9], as well as on geometric aspects such as shape-morphing. Shape-morphing involves the design of structures that are able to change their shape while performing a specific task, in order to improve their characteristics or enable new capabilities. Shape-morphing structures can be found in nature [10], [11] and in engineering fields such as aeronautic [12], [13], deployable structures [14], automobile [15] and architecture [16], [17].

Considerable research has been conducted on the design of binary shape-morphing structures in solids [18], [19], metamaterials [20], [21] as well as origami structures [22]–[24] which are able to follow two shapes during deformation. Research into multi shape-morphing structures that expand upon binary and thus are able to morph into multiple distinct provided shapes is still relatively scarce due to challenges in material limits, added complexity or the absence of knowledge. Recent work in multi shape-morphing includes applications in solids [25], metamaterials [26] and reconfigurable structures [27], [28], but may limit the designer's ability to provide specific objective shapes to the design method for the structure to morph into [28] or have limited applicability. For example, studies into solids designed with topology optimization for multiple designed shapes may be bulky [25] or metamaterial studies in shape-morphing can lack applicability due to scaling issues when unit-cells are assumed to be infinitely small [29]. Further research in multi shape-morphing has the potential to enhance the functionality of a component by expanding its amount of working conditions or reduce its weight by replacing multiple compliant components with a monolithic, more capable component. An interesting area of application for multi shape-morphing structures is in the design of exoskeletons for the human body. Conventional exoskeletons can be either passive [30] or active [31], [32] and rely on rigid beams and springs to acquire their supportive positions. These components can add weight, or introduce the reliance on external power.

The goal of this paper is to expand upon the knowledge of multi shape-morphing by proposing a method for the design of a novel multi shape-morphing structure. This structure is proven to able to morph into multiple distinct shapes and is used for the design of an exoskeleton. This exoskeleton can have potential applications for labor-intensive work by providing a passive back support that is able to be flush with the human body. The proposed structure relies on its geometrically induced stiffness to acquire its multi shape-morphing capability. The design method for this parametric multi shape-morphing structure is able influence the curvature of the structure and thereby influence its local stiffness. This enables the structure to morph into multiple shapes during deformation. The objective of this design method is to compare the shape of the structure on its symmetry plane with a set of objective shapes. It consists of a random search for acquiring a representative sample of the design space, and minimization of the shape error for a set of best designs. Several design cases with different boundary conditions are evaluated as a means to validate the proposed design method. The behavior of these designs is then experimentally validated and sensitivity analyses are performed to identify the relative importance of design variables in relation to the structure's multi shape-morphing performance. The proposed design method is used to design a full-scale prototype exoskeleton based on the shape of the human back in multiple positions. Finally, the results of the study are discussed and an interpretation of the limitations and capabilities of multi shape-morphing is provided.

II. Methodology

In this section, the proposed structure, corresponding design methodology and several design cases for this method are described. Thereafter the design method for an exoskeleton prototype is explained. The used methodology for validation and interpretation of the mechanical behavior of these structures is presented in the form of experimental validation and a sensitivity analysis on relevant design variables.

A. Design functions

In order for the structure to be be used with the following design method and this design method to be able to generate an exoskeleton prototype design, the design needs to have some general characteristics as described in section II-A.

- Be able to elastically deform and approximate a set of input shapes.
- Provide geometric parameters that can be used in optimization.
- Be symmetric.

B. Model

1) Design variables: A parametric beam structure that is able have its shape modified at a given amount of points is constructed. The structure is based on the characteristics from section II-A, and is able to use its shape to influence its bending behavior, similar to a shell structure, but computationally more efficient. This structure is able to exploit its transversal curvature at several locations to influence its deformation behavior. In addition, an additional parameter for shape defined by Y-offset is introduced. This Y-offset will be called frontal offset, and is denoted by Y_d. The transversal curvature is denoted by κ. The structural influence of these design variables is visually represented in fig. 1b. These design variables are constructed for a given amount of design variable sets S that dictate the amount of points where the shape of the structure can be influenced. The usage of these design variable sets is shown in fig. 1a. The design variables are bounded within the ranges of $B_\kappa = (-15\mathrm{m}^{-1}, 15\mathrm{m}^{-1})$ and $B_{Y_d} = (-0.05\mathrm{m}, 0.05\mathrm{m})$. The height of the structure is named L and t_x, t_y and t_z are positional indicators used in discretization of the control point equations, of which the amount of discretized points is given by the designer.

$$f_X(\kappa, t) = \frac{1}{\kappa}\sin t_x \tag{1a}$$

$$f_Y(\kappa, dY, t) = \frac{1}{\kappa}(\cos t_y - 1) - Y_d \tag{1b}$$

$$f_Z(L, t, C) = \frac{t_z L}{S - 1} \tag{1c}$$

The aforementioned variables are used in a set of shape equations described in eqs. (1a) to (1c) are used to define a set of control points.

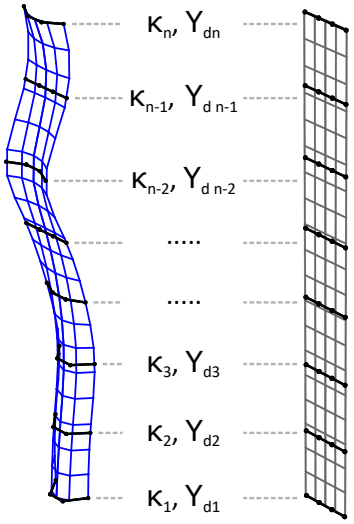

(a) Arbitrarily shaped structure (blue) and neutrally shaped structure (grey) with shape dictated by control points (indicated by black lines) constructed for every design variable set consisting of transversal curvature κ_n and frontal offset Y_d.

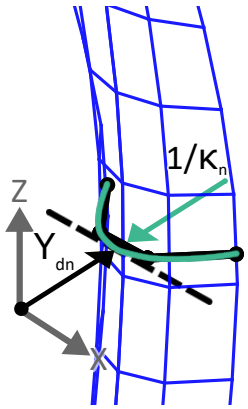

(b) Structural influence of design variables frontal offset Y_d (black arrow) and transversal curvature κ (teal arrow).

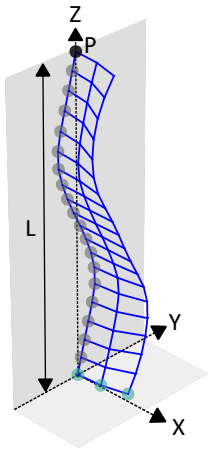

(c) Arbitrary shaped structure of height L with fixed-$\mathbf{C_1}$ (green dots) and symmetry constraints $\mathbf{C_2}$ (grey dots), load point $\mathbf{P}$, ground plane (light grey plane) and symmetry plane (dark grey plane).

Fig. 1: Proposed structure with design variable set methodology (fig. 1a), structural influence of design variables Y_d and κ (fig. 1b), and applied boundary conditions (fig. 1c).

2) Model creation: The geometry of the model is based on a shell surface defined by a set of control points based on eq. (1). This surface is constructed by the use of a Non-Uniform Rational B-spline (NURBS). The coordinates on this two-dimensional plane are described in the U direction and V direction. This surface is then discretized and the amount of nodes in this discretization step is based on a given resolution

for U_{res} and V_{res}. These nodal coordinates are used as beam connection points, and the connected beams form the basis for the used model in fig. 1. The width of the structure (U-direction) is set at 0.1m for a single side, and thus the full width is 0.2m. In most cases, the structural height is set at $L = 1\text{m}$. Every beam in the structure has the same radius r. For this study U_{res} is set to 3 and V_{res} is set to 20, as this provides a good trade-off between computational efficiency and model detail to allow enough degrees of freedom for the structures shape to be altered. Due to the symmetry of the structure and the fact that load conditions are applied in its plane of symmetry, a reduction of the computational load can be realized by evaluating only a single side of the structure.

3) Boundary conditions: As shown in fig. 1c (indicated by grey dots), fixed boundary constraints denoted by $\mathbf{C_1}$ are applied on nodes on the ground plane and symmetry constraints denoted by $\mathbf{C_2}$ (indicated by teal dots) have been placed on the side where the nodes lie on the symmetry plane, except when there is overlap with fixed constraints in which case fixed constraints are dominant. Both of these constraints are described in eq. (2). The structural deformation is evaluated by using a nonlinear Finite Element Method for beams, based on the work of Battini [33]. The material behavior is assumed to be linear-elastic.

$$\mathbf{C} = \begin{bmatrix} X & Y & Z & R_X & R_Y & R_Z \end{bmatrix} \tag{2a}$$

$$\mathbf{C_1} = \begin{bmatrix} 0 & 0 & 0 & 0 & 0 & 0 \end{bmatrix} \tag{2b}$$

$$\mathbf{C_2} = \begin{bmatrix} 0 & F & F & F & 0 & 0 \end{bmatrix} \tag{2c}$$

For the design process of the exoskeleton designs for use with humans, a model describing the approximate trajectory of the attachment point with the human back has been constructed that is to be used as the applied boundary condition. This model can be seen in fig. 4b. This moving attachment point acts as a hinge that therefore does not transfer any induced moment following from its rotation. The hinge position r is defined by L, L_1, L_2, α and timestep fraction i and is given in eq. (3). The values for L_1 and L_2 are chosen such that the resulting circular trajectory of r approximates the attachment point at different stages of deformation of the human back. The Y-position of r_0 is equal to the Y-offset at load point P.

$$L_1 = \frac{7}{20}L \tag{3a}$$

$$L_2 = \frac{13}{20}L \tag{3b}$$

$$r_i = \begin{bmatrix} 0 & L_2 \sin \alpha i & L_1 + L_2 \cos \alpha i \end{bmatrix} \tag{3c}$$

C. Design methodology

1) Objective: The objective of this design method is to find an amount of design variable sets of curvatures κ and frontal offsets Y_d that construct a correctly shaped structure that is able to approximate a set of provided planar objective shapes on its symmetry plane during deformation. This symmetry plane is shown in fig. 2a. The full set of the structural symmetry plane nodes is denoted by $\mathbf{X}$. The full set of planar objective nodes are denoted by $\mathbf{O}$. The amount of objective shapes is denoted by n. For a planar objective shape nodes

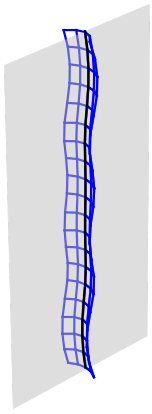

(a) Arbitrary shaped model (blue) with symmetry plane nodes (black) and symmetry plane (grey).

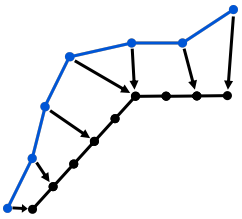

(b) Coupling $\mathbf{X_j}$ (blue) and $\mathbf{O_k}$ (black) based on least distances.

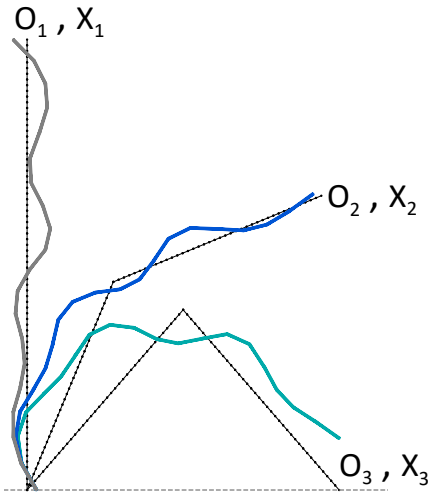

(c) Set of coupled planar objective shape nodes (black dots) denoted by $\mathbf{O_k}$ and symmetry plane nodes (curved lines) denoted by $\mathbf{X_l}$ of arbitrary shaped model.

Fig. 2: Objective function methodology with symmetry plane nodes (fig. 2a), objective and symmetry plane nodes (fig. 2c) and error calculation (fig. 2b).

subset $\mathbf{O_k}$, a subset of symmetry plane shape nodes representing the j-th deformed shape of the structure $\mathbf{X_j}$ is chosen that has the least error between its nodal coordinates $\mathbf{O_k}$ and its corresponding symmetry plane node coordinates $\mathbf{X_j}$ as shown in fig. 2c. Every planar objective shape nodes subset set can only be mapped to a single subset of symmetry plane shape nodes. In order to guarantee a smooth objective function, a sufficient multiple η of objective nodes $\mathbf{o_h}$ are constructed to form every objective node matrix $\mathbf{O_k}$. Therefore, not every objective node is mapped to a symmetry plane node, and thus the structure may be shorter or longer than the given objective

sub shape.

$$\mathbf{x}_i = \begin{bmatrix} X & Y & Z \end{bmatrix}, \quad \mathbf{o}_h = \begin{bmatrix} X & Y & Z \end{bmatrix} \tag{4}$$

$$\mathbf{X_j} = \begin{bmatrix} \mathbf{x}_0 \\ \mathbf{x}_1 \\ . \\ . \\ . \\ \mathbf{x}_{i-1} \\ \mathbf{x}_i \end{bmatrix}, \ \mathbf{O_k} = \begin{bmatrix} \mathbf{o}_1 \\ \mathbf{o}_2 \\ . \\ . \\ . \\ \mathbf{o}_{h-1} \\ \mathbf{o}_h \end{bmatrix}, \ \mathbf{E_j} = \begin{bmatrix} e_0 \\ e_1 \\ . \\ . \\ . \\ e_{i-1} \\ e_i \end{bmatrix} \tag{5}$$

For every deformed node x_i in this set of intermediate nodes on the symmetry plane, an error e_i is defined as the least error value between x_i and every objective node coordinate in $\mathbf{O_k}$, as shown in eq. (6). This value e_i can thus be interpreted an error measure of the coupled structure- and objective node, as shown in fig. 2b. The full error matrix $\mathbf{E_j}$ is then defined as the full set of all the coupled structural nodes with objective nodes in set number j.

$$e_i = \min |\mathbf{x}_i - \mathbf{o}_h| \tag{6}$$

As shown in eq. (7), the norm f_j of the error matrix $\mathbf{E}_j$ representing the coupled intermediate shape node matrix $\mathbf{X}_j$ and corresponding least error objective node matrix $\mathbf{O}_k$ is taken as a sub-metric for the objective function.

$$f_j = |\mathbf{E}_j| \tag{7a}$$

$$\mathbf{F} = [f_0, f_1, \ldots, f_{j-1}, f_j] \tag{7b}$$

The n-minimum values of f_j are taken as a subset of $\mathbf{F}$ as shown in eq. (8), namely $\mathbf{F}_{\text{sub}}$, representing the lowest-error coupled intermediate and objective shapes f_j. The norm of these minimum errors $\mathbf{F}_{\text{sub}}$ over the height of the structure L is then taken as the final objective function F_{obj} as shown in eq. (9).

$$\mathbf{F}_{\text{sub}} = \left\{ \min_n(|\mathbf{F_m}|) \quad | \quad \mathbf{m} = \{1, 2, \ldots, n\} \right\} \tag{8}$$

$$F_{\text{obj}} = \frac{|\mathbf{F}_{\text{sub}}|}{L} \tag{9}$$

2) Random search: In order for the structure to be able to approximate a set of objective shapes, it needs a fair amount of design variable sets. Due to this amount of sets, the design optimization process can involve a large number of design variables and possible combinations, making it infeasible to evaluate the entire design space. Therefore, a random search is conducted to explore a representative subset of the design space. For this study, this sample size is chosen to be $50 \cdot 10^3$. A set of m best performing designs is selected from the random search and used as a starting point for the subsequent minimization process.

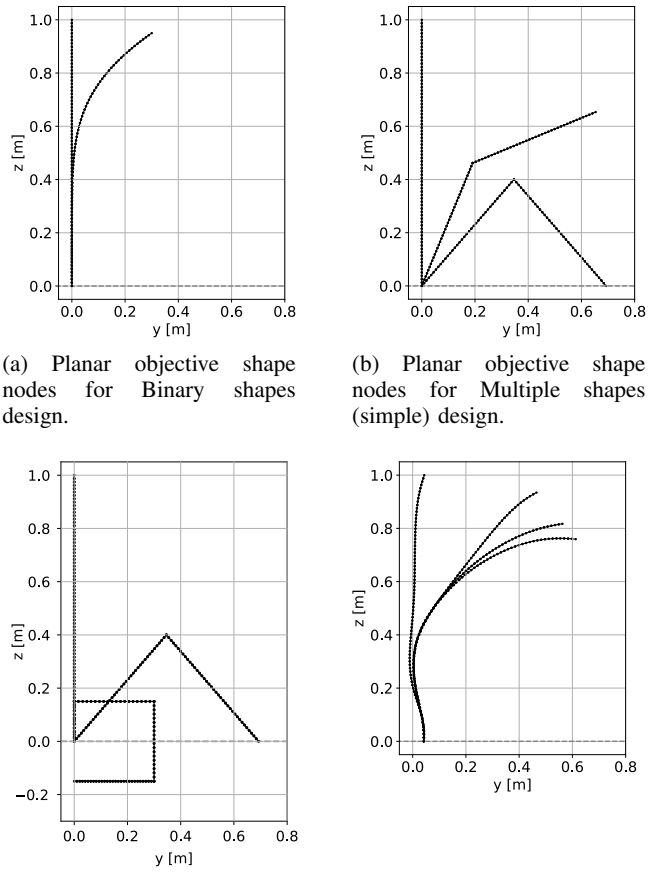

(a) Planar objective shape nodes for Binary shapes design.

(b) Planar objective shape nodes for Multiple shapes (simple) design.

(c) Planar objective shape nodes for Multiple shapes (complex) design.

(d) Planar objective shape nodes for exoskeleton designs.

Fig. 3: Planar objective shapes for the generation of designs.

3) Minimization: The minimization of the error between the design's objective- and symmetry node shapes is performed using the Nelder-Mead method. This method is used to approximate local minima for each design result from the random search. After a set amount of iterations the slope of the objective function is manually evaluated. This process is repeated until a reasonable convergence is reached, at approximately a change in objective function value smaller than $\mathbf{F}_{\text{obj}} = 1 \cdot 10^{-4}\text{m}$. After this minimization, a desirable final design is manually selected based on objective score and load-path characteristic.

4) Design generation: In order to demonstrate the capabilities and effectiveness of the proposed design method to achieve multi shape-morphing, a set of design cases with varying amounts of objective shapes are presented. Two objective shapes is called binary shape-morphing, and anything exceeding this amount is called multi shape-morphing. The binary- and multiple shape design cases serve as generalized applications. The two following designs are generated for the demonstration of the effectiveness of this method for the design of an exoskeleton. All of these examples are described by name, applied boundary condition (B.C.), boundary condition

Design name	B.C.	Value	Shapes
Binary	Y-displacement	0.3m	2
Multiple (simple)	X-rotation	$-\pi\text{rad}$	3
Multiple (complex)	X-rotation	$-\frac{3}{2}\pi\text{rad}$	3
Exoskeleton A	Displaced hinge	$-\frac{5}{18}\pi\text{rad}$	4
Exoskeleton B	Displaced hinge	$-\frac{5}{18}\pi\text{rad}$	4
Prototype	Displaced hinge	$-\frac{5}{18}\pi\text{rad}$	4

TABLE I: Generated designs with their boundary conditions (B.C.) and number of objective shapes.

value and amount of provided objective shapes in table I. The amount of objective shapes ranges from 2 (binary) to 3 or 4 (multiple). The properties described in table II were assigned in to the model for use in simulation.

CS-type	r	E-mod.	C-lines	U-res	V-res	L
Circular	3mm	210 GPa	8	3	20	1 m

TABLE II: Assigned model properties in simulation.

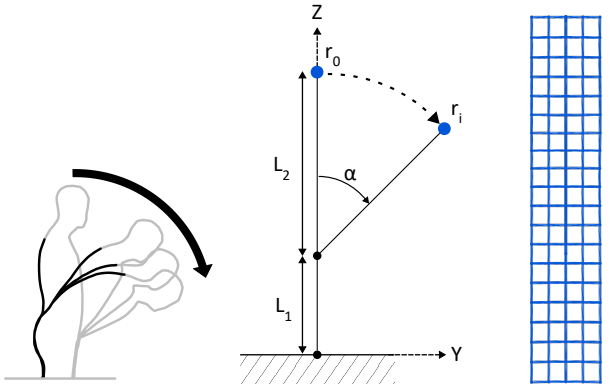

(a) Contours of human back for acquisition of exoskeleton objective shapes.

(b) Model describing the approximate attachment point trajectory (blue dot) as function of α and height L and heights L_1 and L_2.

(c) Front-view of rectangular grid structure based on discretized X-coordinates.

Fig. 4: Acquisition of back shapes (fig. 4a), simplified model of back boundary condition (fig. 4b) and edited model generation for rectangular gird (fig. 4c).

D. Production method

From the proposed exoskeleton designs in table I, four scale models and a full-scale exoskeleton prototype design will be produced. The selected models to be produced can be found in table III.

1) Scale models: The scaled down models as described in table III are produced from Nylon (Nylon 12) with Multi-Jet Fusion and have properties as described in table IV. Multi-jet fusion is a 3D printing technology that utilizes a multi-agent print head system to selectively fuse nylon powder in layers.

Design name	Scale model	Full model
Binary	✓	×
Multiple (Simple)	✓	×
Multiple (Complex)	×	×
Exoskeleton A	✓	×
Exoskeleton B	✓	×
Prototype	×	✓

TABLE III: Produced designs

CS-type	r	E-mod.	C-lines	U-res	V-res	L
Circular	2mm	1.9 GPa	8	3	20	$\frac{1}{3}$m

TABLE IV: Scale model properties.

2) Prototype: As described in section II-A, the design needs to be both flexible and symmetric. In order to produce the design in a fast and geometrically precise fashion, it can be produced in an automated planar fashion and assembled manually. A choice is made for FDM as the production method due to the speed of production and material properties. The use of plastics allows for induced strains up to 6%. This allows the exoskeleton that encounters strains up to 3% to elastically deform instead of plastically. The regular exoskeleton design case from table I was chosen as a starting point for the production process due it having both lower strains and being more stable during deformation as compared to the snap-through exoskeleton design case due to the absence of snap-through behavior.

3) Rectangular design: In order to enable planar production of the exoskeleton, the design was used for an edited model generation that discretizes the X-values of all nodes in the design to a set of given values. The amount of these X-values corresponds to the amount of horizontal nodes given by U_{res}. This discretization set causes the structural grid to be rectangular as shown in fig. 4c. The exoskeleton prototype is designed for the back shapes of the author of this paper as shown in fig. 4a. Therefore, the structural height is set at $0.85m$. The model properties used in simulation for this prototype are shown in table V. The physical version of this prototype has a square cross-section with a width of $3mm$ to aid in manufacturability. Due to this change in height and model generation, the objective score is not near its local minimum. Therefore the design variable set values from the exoskeleton design case were used as an input for an additional minimization run. The result is a similar shaped and performing design.

CS-type	r	E-mod.	C-lines	U-res	V-res	L
Square	3mm	100 MPa	8	3	20	0.85 m

TABLE V: Properties of exoskeleton prototype.

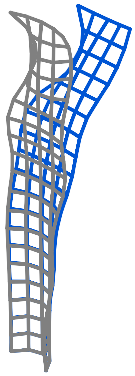

(a) Binary shapes 3D-plot with initial- (grey) and final shape (blue).

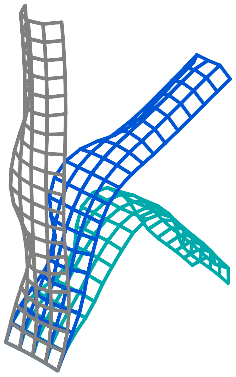

(b) Multiple shapes (simple) 3D-plot with initial- (grey), intermediate- (blue) and final shape (teal).

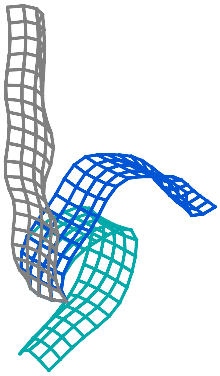

(c) Multiple shapes (complex) 3D-plot with initial- (grey), intermediate- (blue) and final shape (teal).

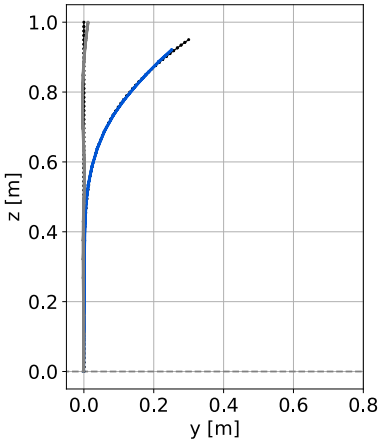

(d) Binary shapes symmetry plane plot with initial- (grey) and final shape (blue) and planar objective shapes (black dotted lines).

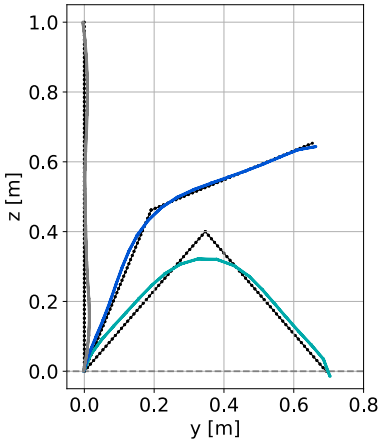

(e) Multiple shapes (simple) symmetry plane plot with initial- (grey), intermediate- (blue) and final shape (teal) and planar objective shapes (black dotted lines).

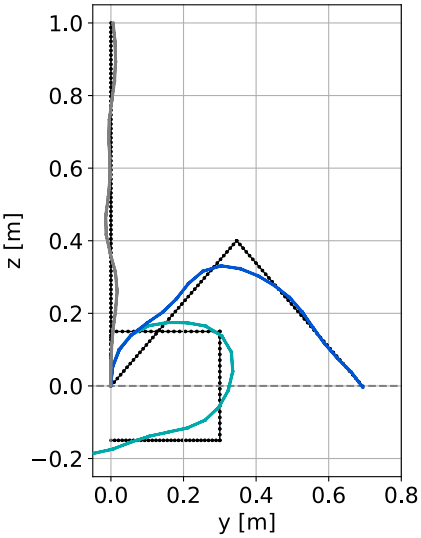

(f) Multiple shapes (complex) symmetry plane plot with initial- (grey), intermediate- (blue) and final shape (teal) and planar objective shapes (black dotted lines).

Fig. 5: Symmetry plane plots and 3D-plots of designs generated with random search and minimization as described in section II-C, ranging from binary (2 shapes) to multiple (3 shapes).

E. Performance validation

The multi shape-morphing performance of all produced models will be assessed by visual measurement of the nodal positions on the symmetry plane and using these symmetry nodes in the objective function as described in section II-C1 to acquire an objective function value. Due to the scale models being smaller, the nodal coordinates will be evenly scaled up to match the simulation height. For the final prototype, the same method will be deployed, but without the scale factor since this is already taken into account as shown in table V. For the binary shapes design, a Y-displacement will be applied by attaching a wire to load point $\mathbf{P}$ and making sure that the wire is kept parallel with the global Y-axis during deformation. For the multiple shapes design, a plastic bellow was used apply a pure rotation on load point $\mathbf{P}$ in order to minimize reaction forces. This bellow has a low stiffness in its radial directions, and a high torsional stiffness. The bellow was kept as straight as possible to minimize reaction forces on the load point. For the exoskeleton designs, the setup from fig. 4b was created using rigid aluminum beams. A similar but scaled up beam frame is used for the evaluation of the full-scale exoskeleton prototype.

F. Sensitivity Analysis

A sensitivity analysis will be performed on all designs for which a model is produced as described in table III. Let $\mathbf{v} = (Y_{d1}, \kappa_1, Y, \kappa_2, \ldots, Y_{dn}, \kappa_n,)$ be a set of design variable values and $F(\mathbf{v})$ be the objective function defined by this set. A step size $\epsilon_{Y_d} = 10^{-6}\mathrm{m}$ or $\epsilon_\kappa = 10^{-6}\mathrm{m}^{-1}$ is taken. The

sensitivity S_i of every design variable in $\mathbf{v}$ with respect to step size ϵ is then given by the forward finite difference equation as given in eq. (10). In this equation, ϵ represents the perturbation being applied to the designated design variable.

$$S_i = \frac{F_{\text{obj}}(v + \epsilon) - F_{\text{obj}}(v)}{\epsilon} \tag{10}$$

This gradient corresponds to the set of sensitivities of each design variable. The interpreted design variables for this analysis values correspond to the found optimal values of the design method from section II-C.

III. Results

A. Design generation

In order to generate designs, the planar objective shapes described in section II-C1 were used as an input for the design method as described in section II-C. The first three will be used to demonstrate the design method. All objective score results from simulation are shown in table VI. Starting with Binary input shapes, as shown in fig. 5a, a binary shape-morphing behavior can be achieved by supplying the design algorithm 2 shapes. The design has a high curvature on its lower region to provide the necessary stiffness to counteract movement, followed by lower curvature areas above, that have lower stiffness and in effect allow more deformation. With multiple input shapes, as shown in fig. 5b, a more simple shape-morphing behavior can be achieved by supplying three shapes. The supplied shapes are in relative proximity to each other during deformation. This design is characterised by a low curvature area on its bottom and middle to allow deformation. As shown in fig. 5c, a more complex shape-morphing behavior is approximated by supplying three shapes that shape-wise are not in relative proximity to each other during deformation.

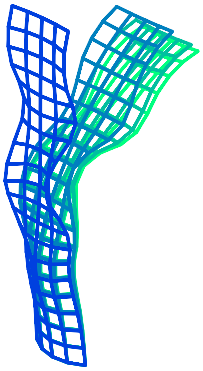

(a) Exoskeleton A design 3D-plot.

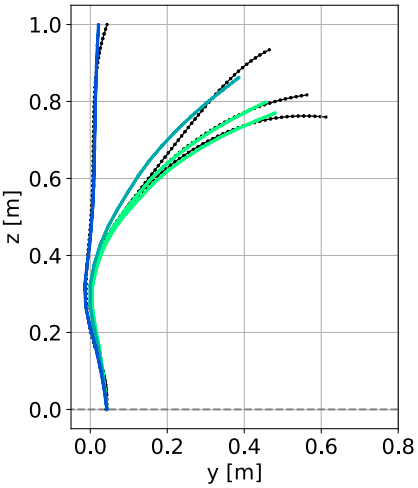

(b) Exoskeleton A design symmetry plane plot with intermediate shapes ranging from blue to green and planar objective shapes (black dotted lines).

Fig. 6: Exoskeleton A design.

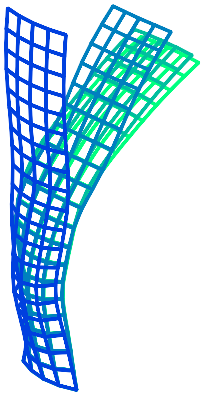

(a) Exoskeleton B design 3D-plot.

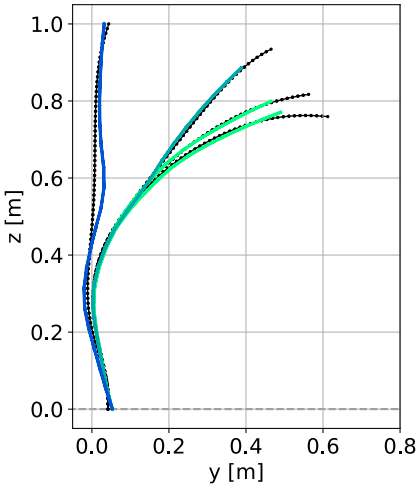

(b) Exoskeleton B design symmetry plane plot with intermediate shapes ranging from blue to green and planar objective shapes (black dotted lines).

Fig. 7: Exoskeleton B design.

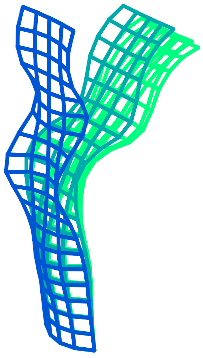

(a) Prototype design 3D-plot.

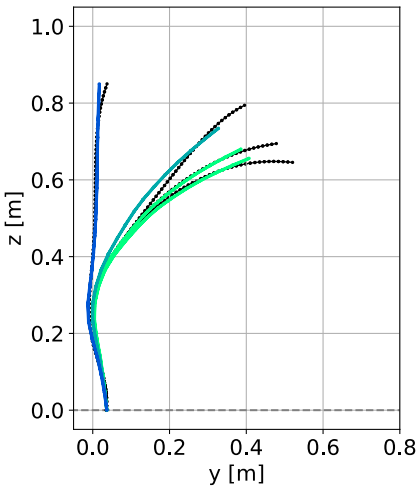

(b) Prototype design symmetry plane plot with intermediate shapes ranging from blue to green and planar objective shapes (black dotted lines).

Fig. 8: Exoskeleton prototype design.

B. Exoskeleton design generation

The measured back shapes of the author of this paper have been obtained and utilized as an input for the design method. Two best-performing cases have been selected and can be seen in figs. 6 and 7. The design in fig. 7 makes use of a different approach and exploits a rapid change in deformation that results in a better objective score. For the full-scale exoskeleton prototype, the model height L has been adjusted to $0,85\text{m}$ in order to fit the authors back. The design from fig. 6 has been chosen as an input and used in an additional minimization run with the rectangular grid model

Design name	Simulated score
Binary Shapes	0,0153
Multiple Shapes (simple)	0,0517
Multiple shapes (complex)	0.101
Exoskeleton A	0,0424
Exoskeleton B	0,0416
Prototype	0,0434

TABLE VI: Objective score results from simulation.

from fig. 4c in order to make the design planar as well as lower in height. The design is shown in fig. 8, and as can be seen the symmetry plane shape is similar to its non-planar counterpart. The Multiple Shape design was loaded with a

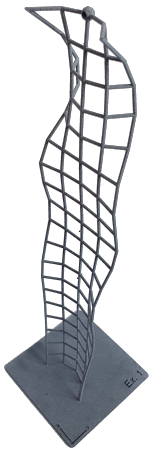

(a) Binary shapes scale model.

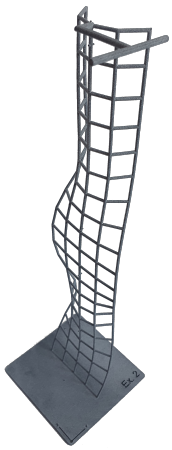

(b) Multiple shapes (simple) scale model.

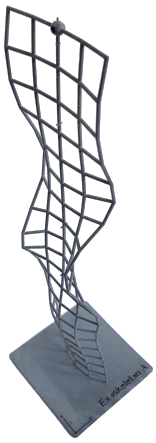

(c) Exoskeleton A scale model.

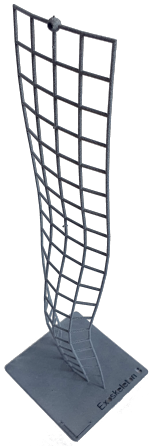

(d) Exoskeleton B scale model.

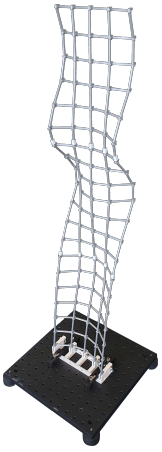

(e) Exoskeleton full-scale prototype.

Fig. 9: Physical nylon scale models produced with Multi-Jet Fusion (figs. 9a to 9d) and physical FDM produced full-scale exoskeleton prototype design (fig. 9e).

rotational constraint as described in table I. The design during deformation is shown in fig. 11.

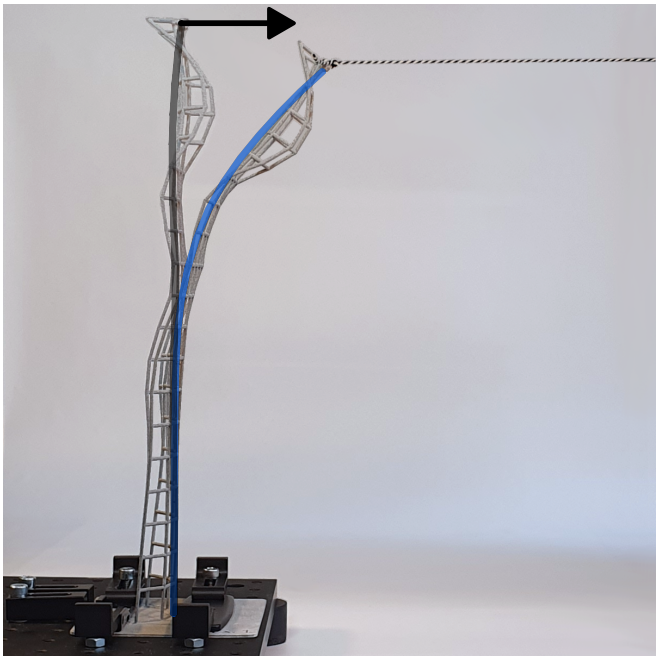

Fig. 10: Binary shapes scale model measurement setup with Y-displacement indicated by arrow → and symmetry plane shape results from simulation consisting of initial- (black) and final shape (blue).

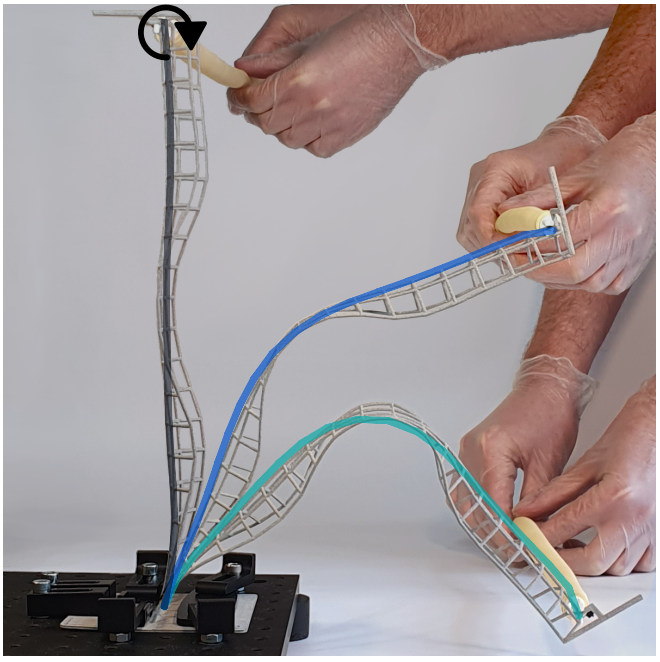

Fig. 11: Multiple shapes (simple) scale model measurement setup with angular displacement indicated by arrow ↷ and symmetry plane shape results from simulation consisting of initial- (black) and intermediate- 1 (blue) and final shape (teal).

C. Experimental validation

The design cases described in table III have been produced. In order to verify the shape-morphing capabilities of

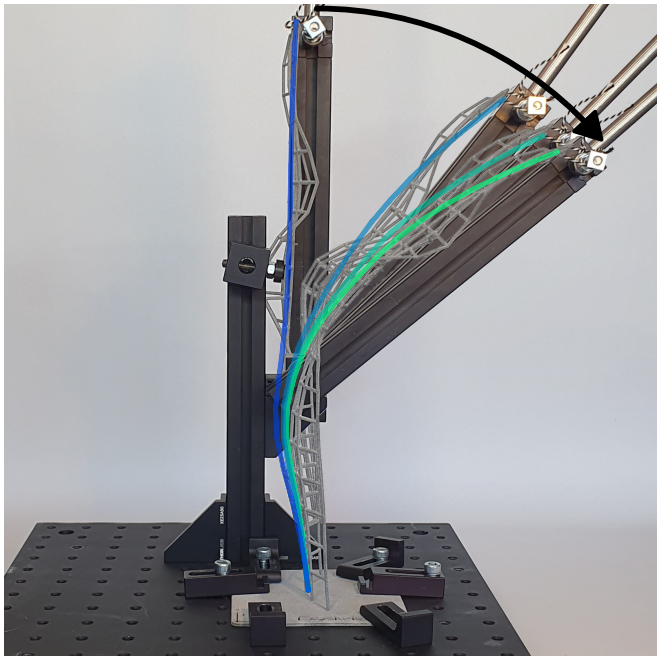

Fig. 12: Exoskeleton A scale model measurement setup with angular displacement indicated by arrow ↷ and symmetry plane shape results from simulation consisting of initial- (black), intermediate- 1 (dark), intermediate- 2 (light), intermediate- 3 (teal) and final shape (green).

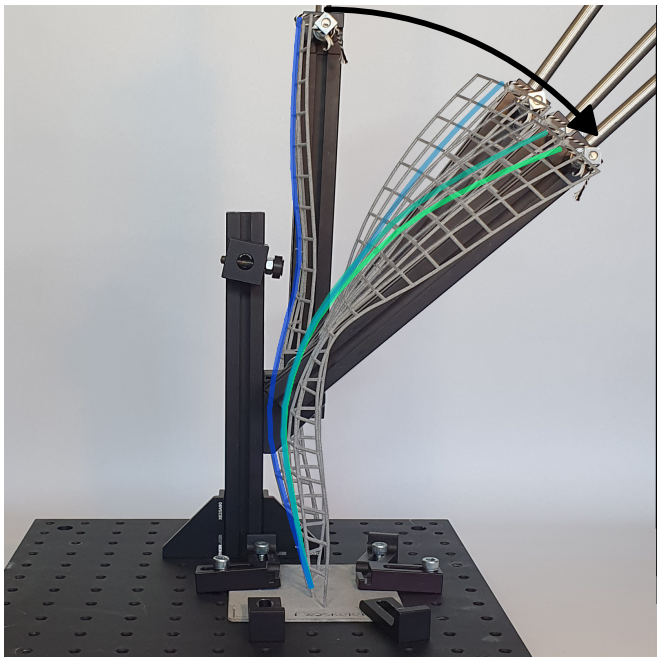

Fig. 13: Exoskeleton B scale model measurement setup with angular displacement indicated by arrow ↷ and symmetry plane shape results from simulation consisting of initial- (black), intermediate- 1 (dark), intermediate- 2 (light), intermediate- 3 (teal) and final shape (green).

the scale models, the scale models have been fixed to a plate and loaded with their respective boundary conditions. Images of the structure in deformation have been un-warped to account for perspective errors and used for visually tracing the symmetry plane node coordinates. The nodal coordinates at the symmetry plane have been normalised for height, and put into the objective function from section II-C in order to make a comparison with the simulation results. These results are shown in table VII, along with their respective simulated scores and their measurement deviation from the simulated score δ. The Binary Shape design during deformation is shown in fig. 10. For both exoskeleton measurements, a high-stiffness beam frame was constructed as described in fig. 1, and used to deform the exoskeleton by pulling it with a short wire. This deformation path represents the attachment point to the human back during deformation. The exoskeleton A design during deformation is shown in fig. 12. The exoskeleton B design during deformation is shown in fig. 13. For the exoskeleton prototype, a similar but larger scale beam frame was constructed and used to deform the exoskeleton. The prototype during deformation is shown in fig. 15.

Design name	Simulated	Measured	δ
Binary Shapes	0,0153	0,0253	0,0100
Multiple Shapes	0,0517	0,0542	0,0025
Exoskeleton A	0,0424	0,0499	0,0076
Exoskeleton B	0,0416	0,0681	0,0265
Prototype	0,0434	0,0516	0,0082

TABLE VII: Objective score results from simulated and measured and difference $\boldsymbol{\delta}$ in objective score for generated designs.

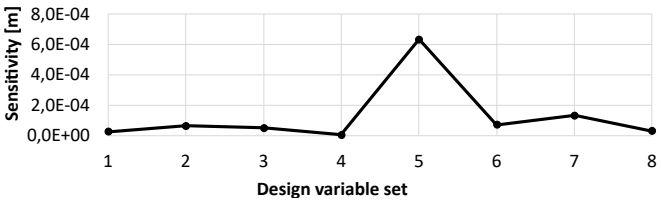

(a) Sensitivity of κ versus design variable set.

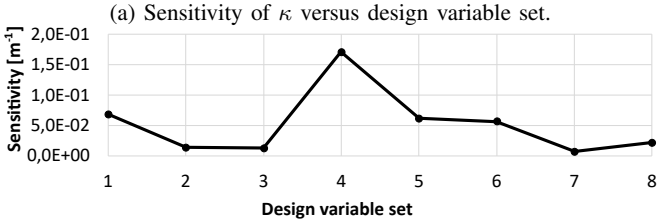

(b) Sensitivity of Y_d versus design variable set.

Fig. 14: Binary shapes design variable sensitivities per set level.

D. Sensitivity Analysis

On each design validated in section II-E, a sensitivity analysis is performed by using a finite difference approximation of the gradient of F. The evaluated design variables are frontal

Fig. 15: Full-scale prototype design based on exoskeleton design case with simulation result shape lines consisting of intermediate- 1 (a, blue), intermediate- 2 (b, light blue), intermediate- 3 (c, teal) and final shape (d, green).

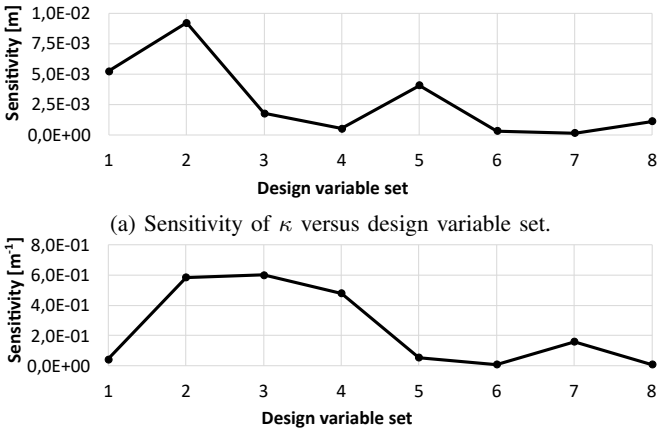

(a) Sensitivity of κ versus design variable set.

(b) Sensitivity of Y_d versus design variable set.

Fig. 16: Multiple shapes (simple) design variable sensitivities per set level.

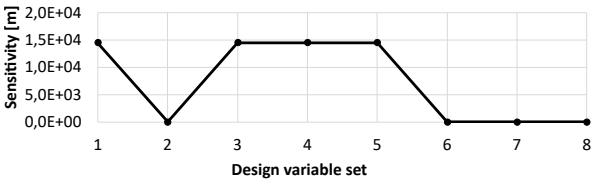

(a) Sensitivity of κ versus design variable set.

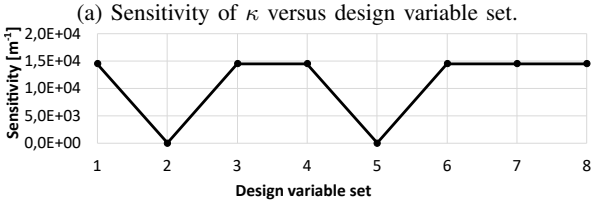

(b) Sensitivity of Y_d versus design variable set.

Fig. 17: Exoskeleton B design variable sensitivities per set level.

offset Y_d and transversal curvature κ. and A step size of $\epsilon = 10^{-6}$m is used for acquiring the gradient. The sensitivities for the binary shapes design can be seen in fig. 14. For both κ and Y_d a peak can be seen at around control point set level 3-4, corresponding to the level where a change from high to low curvature occurs to allow deformation. The sensitivities for the multiple shapes (simple) design are shown in fig. 16. For κ, a peak at the lower- and middle region of the design can be spotted, corresponding to areas with lower stiffness to allow for rotation. For Y_d, the most critical area is between level 0 and 4, corresponding to the area between the two rotational points as given by κ. The sensitivities for the exoskeleton B design can be seen in fig. 17. As can be seen, the design has a high deviation between sensitivities and therefore they can not be used to interpret the structure. The sensitivities for the prototype exoskeleton design can be seen in fig. 19. The sensitivities for the exoskeleton A design can be seen in fig. 18. A high sensitivity of K can be seen on both the fixed end and hinged end of the structure. A peak in Y_d can be seen in the middle of the structure. A second sensitivity analysis has been conducted on the amount of design variable sets that are used to construct the Multiple Shapes (simple) structure. As can be seen in fig. 20, an amount of 4,8 and 12 design

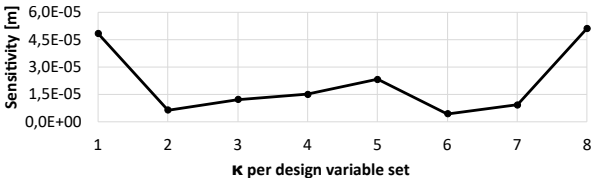

(a) Sensitivity of κ versus design variable set.

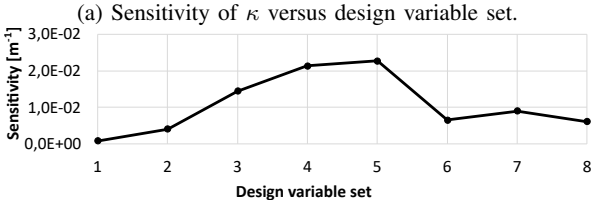

(b) Sensitivity of Y_d versus design variable set.

Fig. 18: Exoskeleton A design variable sensitivities per set level.

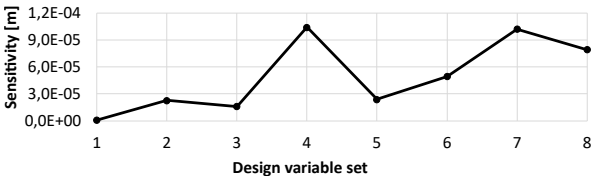

(a) Sensitivity of κ versus design variable set.

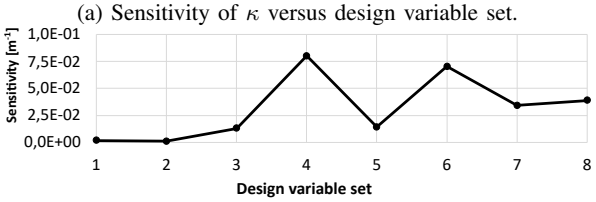

(b) Sensitivity of Y_d versus design variable set.

Fig. 19: Prototype design variable sensitivities per set level.

variable sets have been evaluated for objective score, all with a random search group size of $50 \cdot 10^3$ designs. A fixed amount of $1 \cdot 10^3$ function evaluations were allowed for minimization.

IV. Discussion

A novel design method and parametric structure have been proposed in this paper. This structure is able to exploit its shape in order to influence its bending behavior, and thereby allowing itself to partly morph into a set of provided planar objective shapes. Six designs were constructed, of which four were produced as a scale model and one as an exoskeleton prototype. The deformation of all physical models was experimentally validated, and a sensitivity analysis was performed on these designs.

A. Performance of designs

From the objective score of the binary shapes design it can be concluded that by using the proposed parametric structure and design method, a low error between objective and structural shapes can be achieved for this objective shape set. This proves that two shapes (binary shape-morphing) can be reasonably approximated using the proposed structure. The

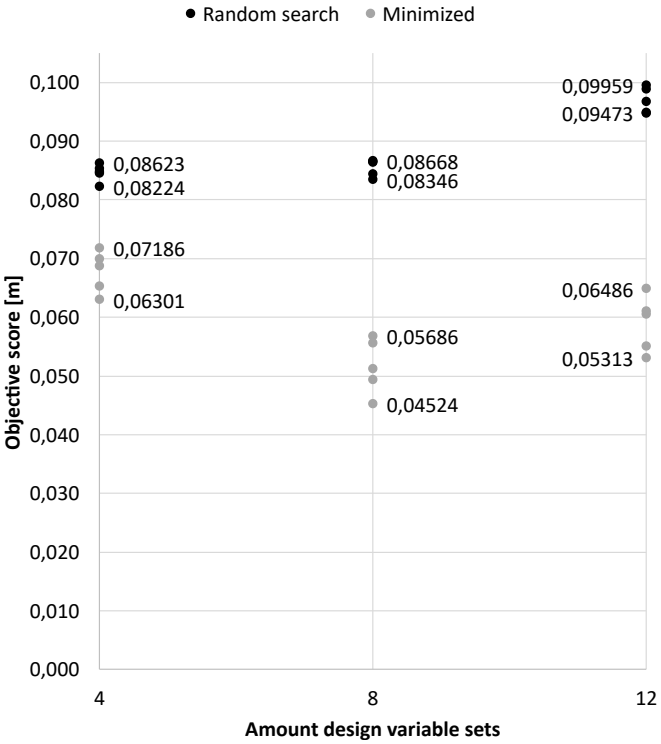

Fig. 20: Top 5 objective scores of $50 \cdot 10^3$ designs for multiple shapes (simple) after random search (black dots) and minimization (grey dots) versus amount of design variable sets.

multiple shapes simple design demonstrates that a low error is also possible for 3 objective shapes, given that these shapes prove to be approximately following a logical deformation path. A limit on this shape-morphing capability is demonstrated by the complex multiple shapes design where the set of 3 objective shapes is too complex for the design method to find a solution. Due to this complexity, the best solution that was found has an objective score of roughly double the score of the other designs. In order to demonstrate the use of the proposed structure for exoskeleton purposes, two designs were proposed. Exoskeleton A is, judging from its objective score and symmetry plane plots, able to approximate a planar shape set consisting of 4 shapes representing the human back in bending over. Both sensitivity analysis and scale model evaluation demonstrate that this design has a higher stability as compared exoskeleton B. The exoskeleton B design proved to be capable of achieving a lower error. The generated design however does so by exploiting an instability which allows it to switch from one to another deformation mode during deformation. This sudden behavior is evaluated to be unstable, as observed in experimental validation as well as in the sensitivity analysis, where a small perturbation causes the design to achieve a drastically higher error. As can be seen in table VI, the prototype exoskeleton has comparable objective score as compared to the non-planar exoskeleton design.

B. Design variable sensitivities

When evaluating the design variable sensitivities for the binary shapes design, a peak in both κ and Y_d representing high sensitivity can be seen. These peaks could correspond to a precision point that serves as an origin to allow the rest of the structure to move about this point. These high sensitivity points are also observed in the multiple shapes design where two peaks of κ are observed that could correspond to the two areas that most allow for deformation in the structure. The sensitivity of Y_d between these two precision points allowing high deformation is observed to be high. This is observed to be attributed to the second precision point and the rest of the structures deformation path being dependent on the deformation accuracy of the first point. For all evaluated structures, it is observed that the sensitivity of Y_d is on average higher than κ. This can be attributed to Y_d having a direct influence on the shape and therefore objective score of the structure during its full deformation range, whereas κ gradually exhibits its influence on the objective score during the deformation of the structure. Another sensitivity analysis has been conducted on the amount of design variable sets that define the shape of the structure. As can be seen in fig. 20, for the evaluated amount of $50 \cdot 10^3$ designs for random search, the objective score does not vary too much from 4 to 8 design variable sets and is sufficient, but for 12 design variable sets the number of evaluated designs is to small. By looking at the random search results for 8 and 12 design variable sets in fig. 20 it is also clear that the found designs for 8 design variable sets are a better starting point for minimization compared to the 12 design variable set random search results when evaluating their minimized score. For an increase in design variables from 8 to 12, a much larger amount of designs would have to be evaluated, which is out of scope for this study due to increased computational time.

C. Design validation

The shape-morphing performance of these designs has been validated experimentally by measuring the symmetry-plane node locations of the produced models under their corresponding boundary conditions during deformation. These node locations have been used to generate an objective score and are compared to the simulation results as a means to verify the shape-morphing performance of the structure. A comparison between simulated-, measured- and difference δ in score can be seen in table VII. For all experimentally validated designs, some errors may be present. Detection errors may be present due to the finite resolution of the camera and occlusion of the symmetry plane by the structure, material errors may arise due to the material not being perfectly homogeneous as assumed and boundary condition errors may be present due to slight inaccuracies in the application. For example, in the Multiple shapes design case, some inaccuracies may be introduced due to the applied rotational boundary condition not being perfect in removing all reaction forces due to manual alignment errors. However, for this design, the difference δ is lower than others which is most likely a result of some reaction forces being applied that have a positive result on the objective score. Exoskeleton B has a bigger deviation than the other designs, this can be attributed to its instability in deformation and tendency to move out of plane when deformed. This behavior was seen during experimental validation and is analogous to a tape spring, as the structure has a convex shape when approached from the negative Y direction. Due to this shape and the applied loading condition, a compressive load will occur in both outermost vertical beams at about half the height of the structure. The out-of-plane instability can be attributed the structure not being perfectly symmetric, which causes one side of the structure to collapse under compression earlier in deformation than the other side. In simulation however, the structure is being evaluated with a symmetric boundary condition. The discrepancy between simulated and experimentally measured objective score can be attributed to the perfect symmetry boundary condition being present in simulation, but not during the experiment. For all produced models, excluding the exoskeleton B, it is observed that the measured (multi) shape-morphing performance is roughly in the same range as the simulated results and therefore, their shape-morphing performance is concluded to be physically viable.

D. Design method

The proposed design method is as stated before, able to generate designs of the proposed structure that approximate the shape sets provided in this paper with a low error. The method enables the designer to evaluate an representative set of possible designs for the given objective shapes, that can be acquired without a lot of prior knowledge of the mechanical behavior of the structure and influence of each design variable. This allows for rapid generation of designs, and to make an assessment of the feasibility of the structure and objective combination. The presented design method does however not guarantee a well-performing solution, since the objective shapes may prove to be incompatible with the structure as well as due to computational constraints due to not being able to fully evaluate the design space for increased resolution and amounts of design variable sets. A consequence of the geometric design freedom is that for the exoskeleton designs generated with the simplified back model, the trajectory can vary between exoskeletons. This is due to the Y-coordinate of the start of the trajectory being matched to the Y-coordinate of the load point. The exoskeleton is able to approximate the objective shapes, but due to the mapping to objective nodes, it can be of different height. Therefore, the load point of the exoskeleton may have a different absolute trajectory for two individual designs, which do not exactly match the height of the attachment point for the human back. This choice for a variable start trajectory is made to allow for the most freedom in design for the proposed method to enable a multi shape-morphing behavior.

E. Capabilities & limits of structure

The multi shape-morphing capability of the proposed model is demonstrated through the manipulation of its geometric

parameters. Several advantages and drawbacks of the presented model can be observed. A drawback of the used model generation technique is that the model is not able to have a different height than specified in order to limit complexity. This height is coupled to the objective shape height, which causes a decrease in the amount of possible solutions. Also, due to the choice for a symmetric structure and planar objective shapes, no boundary conditions that could result in out of plane movement have been evaluated. An advantage of the proposed structure is that the amount of design variable sets can be adjusted, allowing the designer to adjust the geometric complexity of the model to fit their computational constraints. This amount of design variable sets is however limited in control by the topology of the structure, namely the amount of beams in the V direction. The amount of design variable sets must be coupled with the correct amount beams to guarantee that the structure is able to correctly exploit these design variables.

F. Future work

The multi shape-morphing performance of the structure has only been evaluated by use of planar objective shapes. More research could be conducted in adapting the design method to allow for non-planar objective shapes with an extra spatial dimension by the use of B-splines, evaluating the structural shape on multiple planes, or evaluating the whole shape of the structure. Model generation could be altered by enabling the structure to be constructed asymmetrically to further expand the design space. The design space could also be expanded by allowing for a structural height that differs from the objective shape height, to allow for more initial shapes as well as different objective shapes. The multi shape-morphing performance of the structure could be enhanced by introduction of self contact-aided segments [34]–[37] to allow for a varying topology during deformation. These elements can result in a rapid change of stiffness that influences the deformation of the structure as well as the load-path characteristic, and thereby could aid in achieving not only multi shape-morphing but also a more desirable load-path characteristic.

Several aspects of the proposed structure for usage in exoskeleton design could be improved by further research. For example, the bounds of κ could be set such that only a concave or flat structure could be generated. This would be beneficial for the structure being flush with the human back, but would however decrease the design space and could increase the chance of instability based designs being generated. An improvement for additional stiffness of the structure could be introduced by changing the topology of the structure by increasing U_{res}. This would increase the stiffness by addition of vertical elements, at the cost of an increase in computational time. Other means of increasing the stiffness of the structure could be by evaluating different types of materials than the one in this paper, that posses a similar high elastic strain limit but an increase in stiffness, such as titanium.

V. Conclusion

A novel design method is presented for acquiring multi shape-morphing behavior with the accompanying parametric beam structure. The proposed design method is able to influence the shape of the structure at multiple locations to allow for it to morph into multiple shapes when deformed. Multiple designs were generated and their mechanical behavior was validated experimentally. A sensitivity analysis was performed on the design variables of most of the designs, as well as on the amount of design variables necessary for a fixed simulation time.

The results of the experimental validation of the designs proved to be comparable to the simulated results, verifying the capabilities of the structure. The sensitivity analysis on design variables identified some sections in each design that were the most sensitive for small changes. The sensitivity analysis on the amount of design variables proved that a correct group size for the amount of design variables was used.

Overall, it is concluded that not only shape-morphing but multi shape-morphing is possible with the provided structure, given some limits to the complexity of the provided objective shapes. It is concluded that the proposed design method able to generate designs of the proposed structure that approximate the shape sets provided in this paper with a low error to allow the multi shape-morphing capabilities. The design method allows for evaluating the capabilities of the structure without too much prior knowledge about the mechanical behavior of the structure, but does not guarantee a solution within the design space. The design space is however limited by the limited amount of geometric design variables such as structural height or required symmetry.

Further research into the multi shape-morphing capabilities of the proposed structure could benefit from the introduction of asymmetric structures, different topologies or a more comprehensive evaluation of the shape of the structure. Further research into multi shape-morphing could allow for a new generation of structures or mechanisms that are more capable in function or more efficient in weight.

References

[1] T. Lourdes Thomas, V. Kalpathy Venkiteswaran, G. K. Ananthasuresh, and S. Misra, "Surgical Applications of Compliant Mechanisms: A Review," 4 2021.

[2] S. Kota, J. Joo, Z. Li, S. M. Rodgers, and J. Sniegowski, "Design of Compliant Mechanisms: Applications to MEMS," Tech. Rep., 2001.

[3] R. M. Fowler, L. L. Howell, and S. P. Magleby, "Compliant space mechanisms: A new frontier for compliant mechanisms," *Mechanical Sciences*, vol. 2, no. 2, pp. 205–215, 2011.

[4] L. L. Howell, "Compliant Mechanisms," in *21st Century Kinematics*. Springer London, 2013, pp. 189–216.

[5] O. Sigmund, "On the design of compliant mechanisms using topology optimization," *Mechanics of Structures and Machines*, vol. 25, no. 4, pp. 493–524, 1997.

[6] J. A. Gallego and J. Herder, "Synthesis methods in compliant mechanisms: An overview," Tech. Rep. PARTS A AND B, 2009.

[7] M. I. Frecker, G. K. Ananthasuresh, S. Nishiwaki, N. Kikuchi, and S. Kota, "Topological synthesis of compliant mechanisms using multi-criteria optimization," Tech. Rep. 2, 1997.

[8] A. Saxena and G. K. Ananthasuresh, "Topology synthesis of compliant mechanisms for nonlinear force–deflection and curved path specifications," *Journal of Mechanical Design, Transactions of the ASME*, vol. 123, no. 1, pp. 33–42, 3 2001.

[9] L. L. Howell and A. Midha, "A method for the design of compliant mechanisms with small-length flexural pivots," *Journal of Mechanical Design, Transactions of the ASME*, vol. 116, no. 1, pp. 280–290, 1994.

[10] V. Charpentier, P. Hannequart, S. Adriaenssens, O. Baverel, E. Viglino, and S. Eisenman, "Kinematic amplification strategies in plants and engineering," 5 2017.

[11] S. Li and K. W. Wang, "Plant-inspired adaptive structures and materials for morphing and actuation: A review," *Bioinspiration and Biomimetics*, vol. 12, no. 1, 2 2017.

[12] S. Vasista, O. Mierheim, and M. Kintscher, "Morphing Structures, Applications of," in *Encyclopedia of Continuum Mechanics*. Springer Berlin Heidelberg, 2019, pp. 1–13.

[13] Y. Zhang, W. Ge, Z. Zhang, X. Mo, and Y. Zhang, "Design of compliant mechanism-based variable camber morphing wing with nonlinear large deformation," *International Journal of Advanced Robotic Systems*, vol. 16, no. 6, 11 2019.

[14] A. Yellowhorse, J. Rommers, A. Amoozandeh, and J. L. Herder, "Methods for shape fitting in morphing compliant mechanisms," Tech. Rep., 2021.

[15] S. Daynes and P. M. Weaver, "Review of shape-morphing automobile structures: Concepts and outlook," Tech. Rep. 11, 2013.

[16] F. Fiorito, M. Sauchelli, D. Arroyo, M. Pesenti, M. Imperadori, G. Masera, and G. Ranzi, "Shape morphing solar shadings: A review," pp. 863–884, 3 2016.

[17] Y. Li, Y. Zhao, Y. Chi, Y. Hong, and J. Yin, "Shape-morphing materials and structures for energy-efficient building envelopes," 12 2021.

[18] K. J. Lu and S. Kota, "Design of compliant mechanisms for morphing structural shapes," *Journal of Intelligent Material Systems and Structures*, vol. 14, no. 6, pp. 379–391, 2003.

[19] A. Albanesi, F. Bre, V. Fachinotti, and C. Gebhardt, "Simultaneous ply-order, ply-number and ply-drop optimization of laminate wind turbine blades using the inverse finite element method," *Composite Structures*, vol. 184, pp. 894–903, 1 2018.

[20] C. Jiang, F. Rist, H. Wang, J. Wallner, and H. Pottmann, "Shape-morphing mechanical metamaterials," *CAD Computer Aided Design*, vol. 143, 2 2022.

[21] A. Rafsanjani and D. Pasini, "Bistable auxetic mechanical metamaterials inspired by ancient geometric motifs," *Extreme Mechanics Letters*, vol. 9, pp. 291–296, 12 2016.

[22] G. P. Choi, L. H. Dudte, and L. Mahadevan, "Compact reconfigurable kirigami," *Physical Review Research*, vol. 3, no. 4, pp. 1–16, 2021.

[23] S. Li and K. W. Wang, "Fluidic origami: A plant-inspired adaptive structure with shape morphing and stiffness tuning," *Smart Materials and Structures*, vol. 24, no. 10, 9 2015.

[24] S. R. Woodruff and E. T. Filipov, "Bending and twisting with a pinch: Shape morphing of creased sheets," *Extreme Mechanics Letters*, vol. 52, 4 2022.

[25] S. Kirmse, L. F. Campanile, and A. Hasse, "Synthesis of compliant mechanisms with selective compliance – An advanced procedure," *Mechanism and Machine Theory*, vol. 157, 3 2021.

[26] K. Che, C. Yuan, J. Wu, H. J. Qi, and J. Meaud, "Three-dimensional-printed multistable mechanical metamaterials with a deterministic deformation sequence," *Journal of Applied Mechanics, Transactions ASME*, vol. 84, no. 1, 1 2017.

[27] W. Liu, H. Jiang, and Y. Chen, "3D Programmable Metamaterials Based on Reconfigurable Mechanism Modules," *Advanced Functional Materials*, vol. 32, no. 9, 2 2022.

[28] J. T. Overvelde, J. C. Weaver, C. Hoberman, and K. Bertoldi, "Rational design of reconfigurable prismatic architected materials," *Nature*, vol. 541, no. 7637, pp. 347–352, 1 2017.

[29] F. Wenz, I. Schmidt, A. Leichner, T. Lichti, S. Baumann, H. Andrae, and C. Eberl, "Designing Shape Morphing Behavior through Local Programming of Mechanical Metamaterials," *Advanced Materials*, vol. 33, no. 37, 9 2021.

[30] T. Bosch, J. van Eck, K. Knitel, and M. de Looze, "The effects of a passive exoskeleton on muscle activity, discomfort and endurance time in forward bending work," *Applied Ergonomics*, vol. 54, pp. 212–217, 5 2016.

[31] P. N. Kooren, J. Lobo-Prat, A. Q. Keemink, M. M. Janssen, A. H. Stienen, I. J. de Groot, M. I. Paalman, R. Verdaasdonk, and B. FJM Koopman, "Design and Control of the Active A-Gear: a Wearable 5 DOF Arm Exoskeleton for Adults with Duchenne Muscular Dystrophy*," Tech. Rep.

[32] K. Nizamis, A. H. A. Stienen, D. G. Kamper, T. Keller, D. H. Plettenburg, E. J. Rouse, D. Farina, B. F. J. M. Koopman, and M. Sartori, "Transferrable Expertise From Bionic Arms to Robotic Exoskeletons: Perspectives for Stroke and Duchenne Muscular Dystrophy," *IEEE Transactions on Medical Robotics and Bionics*, vol. 1, no. 2, pp. 88–96, 4 2019.

[33] J.-M. Battini and C. Pacoste, "Co-rotational beam elements with warping effects in instability problems," Tech. Rep. [Online]. Available: www.elsevier.com/locate/cma

[34] M. Jin, B. Zhu, J. Mo, Z. Yang, X. Zhang, and L. L. Howell, "A CPRBM-based method for large-deflection analysis of contact-aided compliant mechanisms considering beam-to-beam contacts," *Mechanism and Machine Theory*, vol. 145, p. 103700, 2020. [Online]. Available: https://doi.org/10.1016/j.mechmachtheory.2019.103700

[35] V. Mehta, M. Frecker, and G. Lesieutre, "Contact-aided compliant mechanisms for morphing aircraft skin," in *Modeling, Signal Processing, and Control for Smart Structures 2008*, vol. 6926. SPIE, 3 2008, p. 69260C.

[36] Y. Tummala, A. Wissa, M. Frecker, and J. E. Hubbard, "Design and optimization of a contact-aided compliant mechanism for passive bending," *Journal of Mechanisms and Robotics*, vol. 6, no. 3, 6 2014.

[37] B. Hargrove, A. Nastevska, M. Frecker, and J. Jovanova, "Pseudo Rigid Body Model for Nonlinear Folding Contact-Aided Compliant Mechanism," *SSRN Electronic Journal*, no. 1, 2022.

A

Supplementary material: Design variables

A.1. Bounds

For both design variables that can influence the shape of the structure at levels dictated by the amount of design variable sets, bounds have been set up to limit the design space. For setting up bounds for K, the width of the structure is taken to be $w_{\text{full}} = 0.2$m, therefore $w_{\text{side}} = 0.1$m. Values of K should not allow local curvature of the structure with an end-angle past $\theta = 90°$. In the circle circumference equation from equation (A.1), w_{side} and θ can be plugged in to acquire appropriate limits for r. Thereafter, κ can be acquired as shown in equation (E.1). An absolute limit for κ of 15.708 is acquired, which is rounded to $\kappa = 15\text{m}^{-1}$. In order to allow both positive and negative values for κ, the lower limit has been set to -15m^{-1}, and higher limit to 15m^{-1}. It is important to note that whenever a value of κ is evaluated that is within an absolute threshold of $c = 10^{-6}\text{m}^{-1}$, κ is set to c in order to prevent unnecessary large numerical values for r in model generation.

$$l_{\text{side}} = \theta r \tag{A.1}$$

$$\kappa = \frac{1}{r} \tag{A.2}$$

For the second design variable in each design variable set, the lower and upper bounds for Y_d were set to allow for 5% of the original simulation height L of the structure. Therefore the lower and upper bounds are set to -0.05m and 0.05m respectively.

A.2. Numerical values

In this subsection, the found design variable values for each generated design in the research paper are stated. For readability, alongside the found values is a copy of a 3D-plot and the corresponding symmetry plane node plot from the research paper.

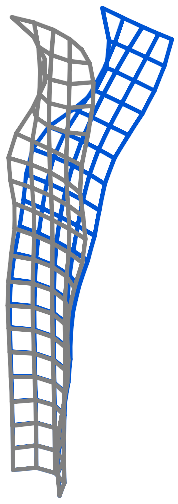

(a) 3D-plot with initial- (grey) and final shape (blue).

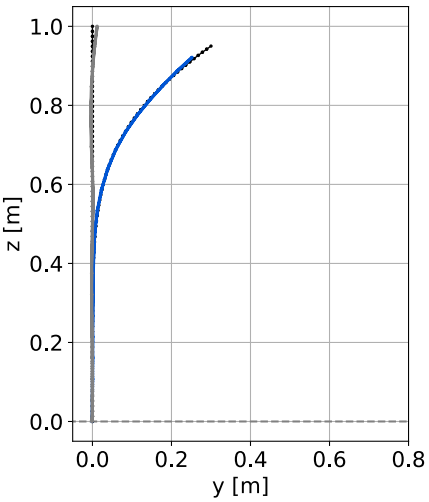

(b) Symmetry plane plot with initial- (grey) and final shape (blue) and planar objective shapes (black dotted lines).

Level	Y_d	K
1	-0.00704	14.54271
2	-0.00762	14.75581
3	-0.00353	9.82769
4	-0.00358	9.25759
5	-0.00228	1.63895
6	0.00145	2.99332
7	0.01012	-14.96644
8	-0.01416	4.30499

(c) Binary shapes design variable values from bottom of structure to top.

Figure A.1: Binary shapes 2D (figure A.1a) and 3D (figure A.1b) plots and corresponding design variables (table A.1c) per set level.

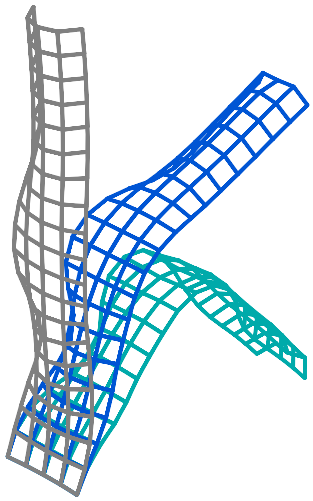

(a) 3D-plot with initial- (grey), intermediate (blue) and final shape (teal).

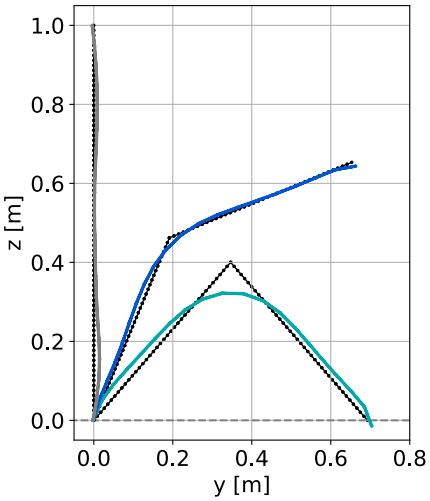

(b) Symmetry plane plot with initial- (grey), intermediate (blue) and final shape (teal) and planar objective shapes (black dotted lines).

Level	Y_d	K
1	0.00168	0.92139
2	-0.01091	-6.3108
3	0.00033	-14.93151
4	-0.0006	-4.90884
5	0.00166	-6.26096
6	-0.00039	-12.49174
7	0.00029	-14.99875
8	0.01212	-14.99997

(c) Multiple shapes (simple) design variable values.

Figure A.2: Multiple shapes (simple) 2D (figure A.2a) and 3D (figure A.2b) plots and corresponding design variables (table A.2c) per set level.

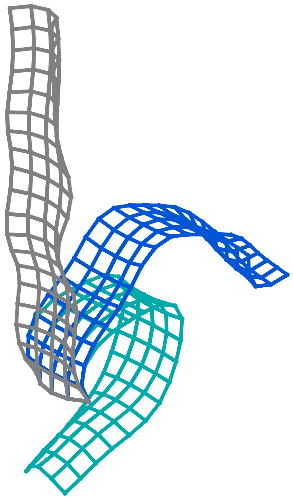

(a) 3D-plot with initial- (grey), intermediate (blue) and final shape (teal).

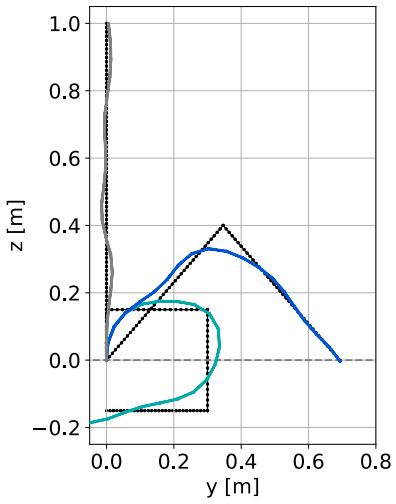

(b) Symmetry plane plot with initial- (grey), intermediate (blue) and final shape (teal) and planar objective shapes (black dotted lines).

Level	Y_d	K
1	0.00504	-8.47951
2	-0.00792	5.93159
3	-0.01917	5.68741
4	0.00846	10.13153
5	0	4.61184
6	-0.00022	10.47662
7	-0.01942	15
8	-0.0142	15

(c) Multiple shapes (complex) design variable values.

Figure A.3: Multiple shapes (complex) 2D (figure A.3a) and 3D (figure A.3b) plots and corresponding design variables (table A.3c) per set level.

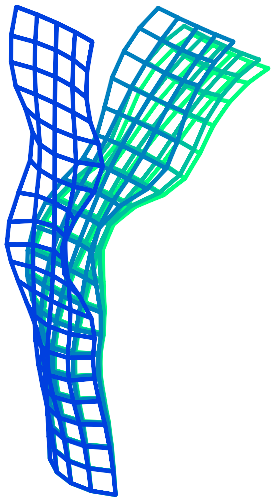

(a) 3D-plot with intermediate shapes ranging from blue to teal.

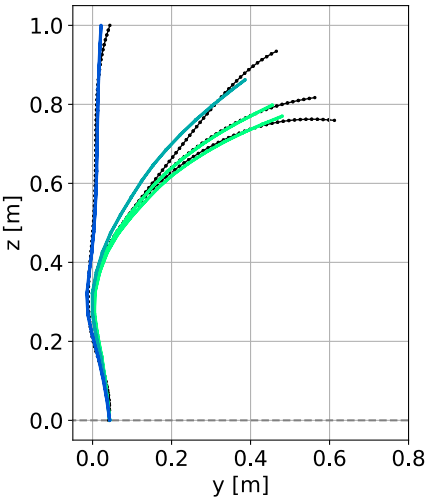

(b) Symmetry plane plot with intermediate shapes ranging from blue to teal and planar objective shapes (black dotted lines).

Level	Y_d	K
1	-0.03916	-7.38059
2	-0.01239	-10.48991
3	0.02147	-13.59662
4	0.00324	-1.47302
5	-0.01372	13.74444
6	-0.00315	-7.33619
7	-0.00893	2.49281
8	-0.01162	1.50367

(c) Exoskeleton A design variable values.

Figure A.4: Exoskeleton A 2D (figure A.4a) and 3D (figure A.4b) plots and corresponding design variables (table A.4c) per set level.

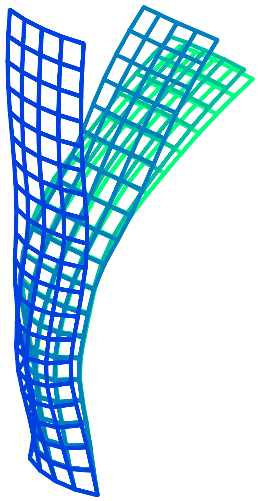

(a) 3D-plot with intermediate shapes ranging from blue to teal.

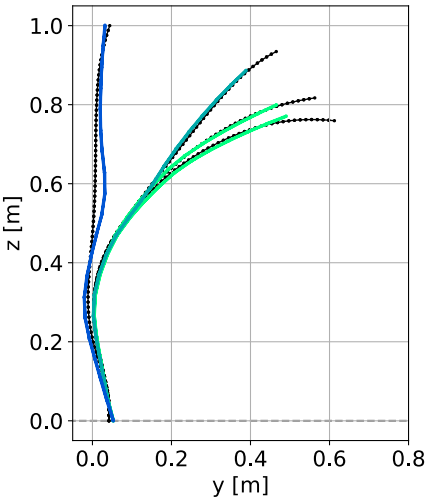

(b) Symmetry plane plot with intermediate shapes ranging from blue to teal and planar objective shapes (black dotted lines).

Level	Y_d	K
1	-0.05	-5.09453
2	0.00035	-14.22102
3	0.03399	-14.93024
4	0.01229	-8.70034
5	-0.01911	-4.22911
6	-0.00371	-4.88939
7	0.00221	-3.23189
8	-0.00058	-2.80954

(c) Exoskeleton B design variable values.

Figure A.5: Exoskeleton B 2D (figure A.5a) and 3D (figure A.5b) plots and corresponding design variables (table A.5c) per set level.

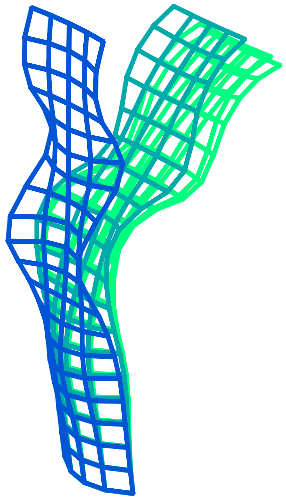

(a) 3D-plot with intermediate shapes ranging from blue to teal.

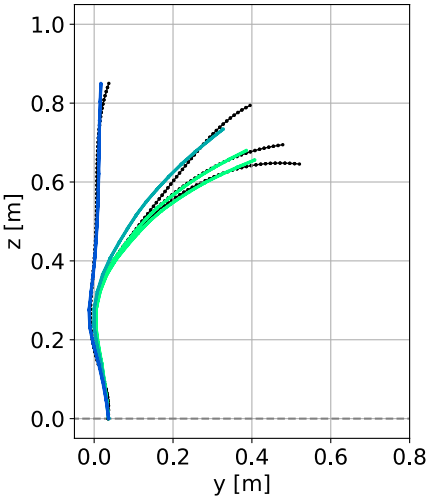

(b) Symmetry plane plot with intermediate shapes ranging from blue to teal and planar objective shapes (black dotted lines).

Level	Y_d	K
1	-0.03235	-7.77545
2	-0.01032	-9.61898
3	0.01991	-13.73947
4	0.00308	0.00378
5	-0.01338	14.77522
6	-0.00247	-9.74619
7	-0.00921	2.78218
8	-0.0099	1.03608

(c) Prototype design variable values.

Figure A.6: Prototype 2D (figure A.6a) and 3D (figure A.6b) plots and corresponding design variables (table A.6c) per set level.

B

Supplementary material: Reaction force and moments

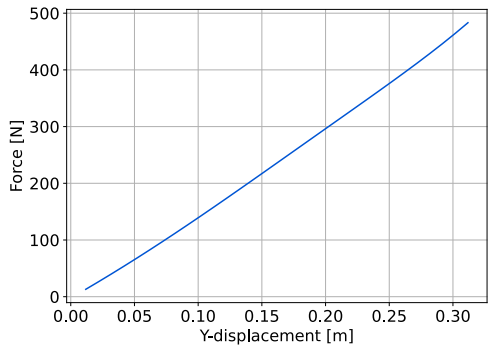

(a) Binary shape morphing force-deflection diagram.

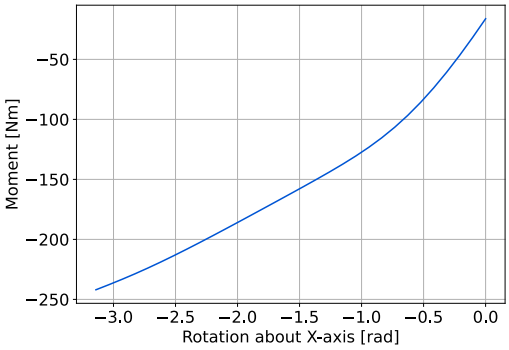

(b) Multiple shapes (simple) moment-angle diagram.

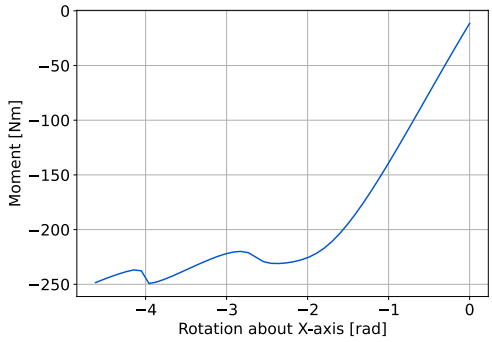

(c) Multiple shapes (complex) moment-angle diagram.

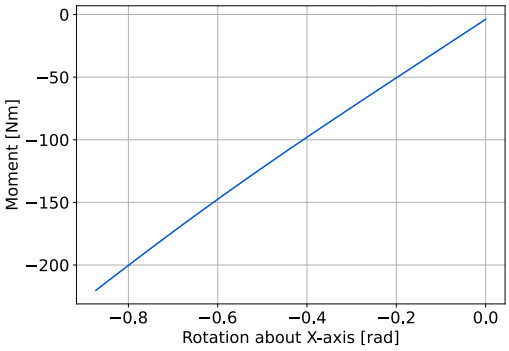

(d) Exoskeleton A moment-angle diagram.

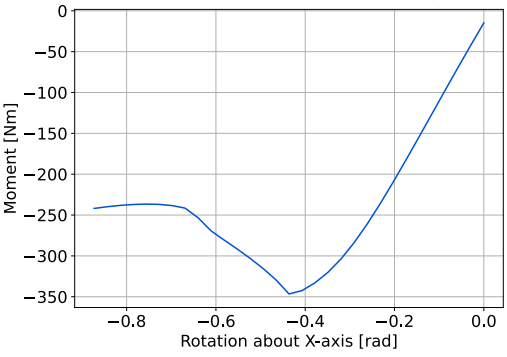

(e) Exoskeleton B moment-angle diagram with rotation applied at pulling beam from simplified back model.

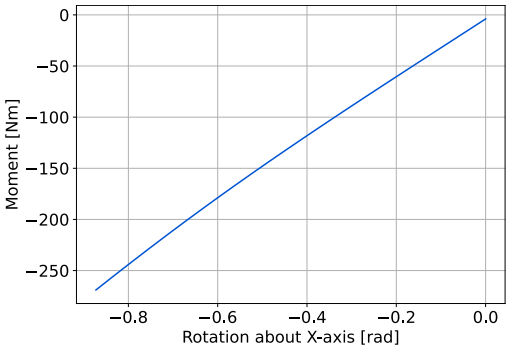

(f) Prototype exoskeleton moment-angle diagram with rotation applied at pulling beam from simplified back model.

Figure B.1: Reaction force and moments at load point P of the structure versus the applied boundary condition per design case.

For each of the design cases in the research paper(figure 2.1), the corresponding reaction force- and moment graphs are shown in figure B.1. Since the applied rotations for all the design cases based on a rotational boundary condition are in the negative direction, their corresponding reaction moments are also negative. As can be seen in figure B.1c and figure B.1e, due to the present instabilities there are introduced nonlinearities in the behavior of the structure.

C

Supplementary material: Varying radius and topologies

C.1. Influence of increase in radius

The stiffness of a single beam consists of an inertia term that includes r^4, as shown in equation (C.1). Therefore, the radius of the beams can be used to tune the stiffness of the structure. By increasing the radius, usually a scalar multiplication of the force-deflection or moment-angle behavior can be achieved.

$$I_{yy} = I_{zz} = \frac{\pi r^4}{4} \tag{C.1}$$

C.2. Varying topologies

As shown in figure C.1, the topology of the structure can be varied in U-direction (horizontal) and V-direction (vertical) to alter the behavior of the structure under load. For demonstration, multiple structures with varying properties are loaded with a Y-displacement of 0.28m. In figure C.2 the structure has $r = 3$ and $\kappa = 0\text{m}^{-1}$. In figure C.4 the structure has $r = 3$ and $\kappa = 5\text{m}^{-1}$. In figure C.3 the structure has $r = 6$ and $\kappa = 0\text{m}^{-1}$. In figure C.5 the structure has $r = 6$ and $\kappa = 5\text{m}^{-1}$. For figure C.2 and figure C.3, the radius has been doubled. By measuring the force at figure C.2b (39.8m) and comparing it to figure C.3b, it can indeed be concluded that $39.8N \cdot 2^4 \approx 636.5N$. When comparing the curved structures from figure C.4 and figure C.5, a change in deformation behavior can be seen. This change can most likely be attributed due to the increase of radius r, as the structure is less prone to exhibit snap-through behavior in figure C.5. As can be seen in figure C.2a and figure C.3a, when no curvature is present in the system, there is no sensitivity to an increase in the amount of horizontal segments defined by U_{res}. This can be explained by the absence of compressive or tensile forces in the structure due to the absence of curvature. Furthermore, by comparing figure C.2 and figure C.4, the effect of curvature can be identified to be very influential in increasing the stiffness of the structure.

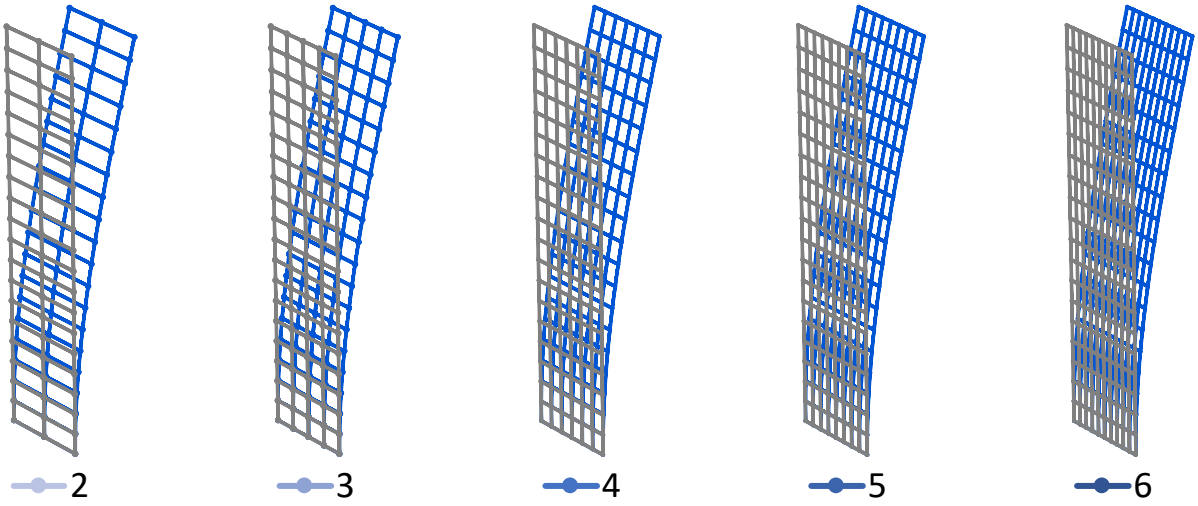

(a) Varying values of U_{res} ranging from 2 to 6 and V_{res} fixed at 20.

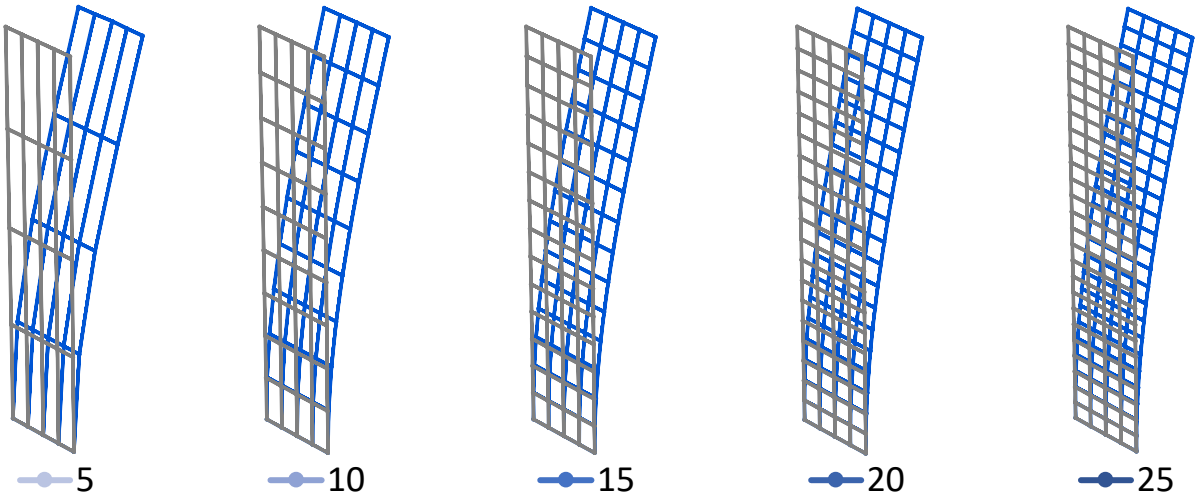

(b) Varying values V_{res} from 5 to 25 and U_{res} fixed at 3.

Figure C.1: Initial (grey) and deformed (blue) structure with fixed radius and varying topology due to alteration of U_{res} (figure C.1a) and V_{res} (figure C.1b) and their respective resolution values and color labels.

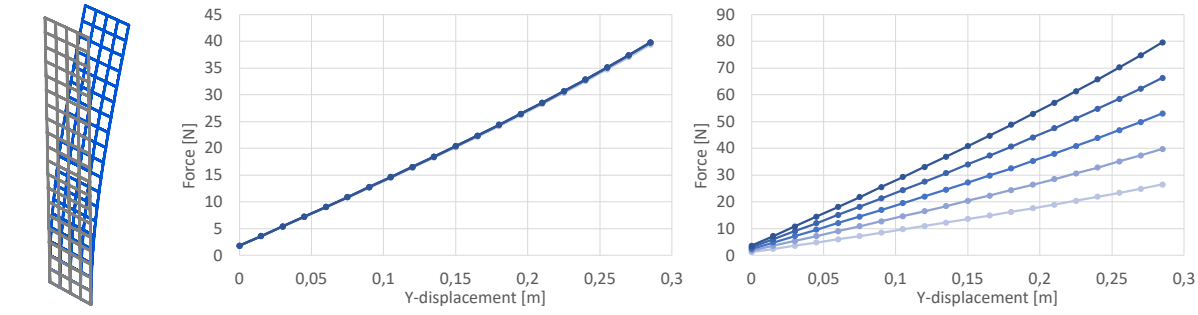

(a) Structure model. **(b)** Force deflection for varying values of V_{res}. **(c)** Force deflection for varying values of U_{res}.

Figure C.2: Model and force-deflection graphs of structure with beam-radius of 3mm, $\kappa = 0\text{m}^{-1}$, and varying values of U_{res} (figure C.2b) and V_{res} (figure C.2c).

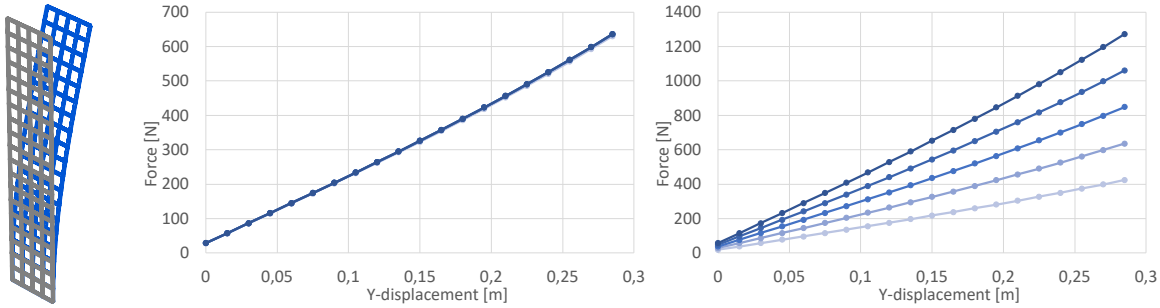

(a) Structure model. **(b)** Force deflection for varying values of V_{res}. **(c)** Force deflection for varying values of U_{res}.

Figure C.3: Model and force-deflection graphs of structure with beam-radius of 6mm, $\kappa = 0\text{m}^{-1}$, and varying values of U_{res} (figure C.3b) and V_{res} (figure C.3c).

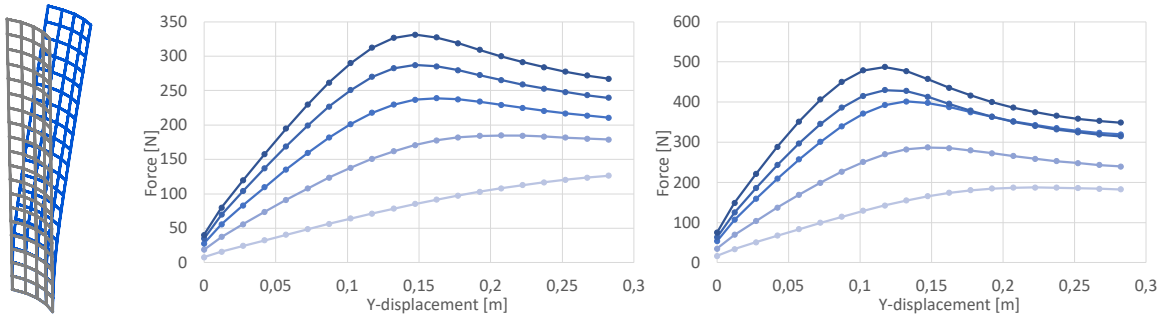

(a) Structure model. **(b)** Force deflection for varying values of V_{res}. **(c)** Force deflection for varying values of U_{res}.

Figure C.4: Model and force-deflection graphs of structure with beam-radius of 3mm, $\kappa = 5\text{m}^{-1}$, and varying values of U_{res} (figure C.4b) and V_{res} (figure C.4c).

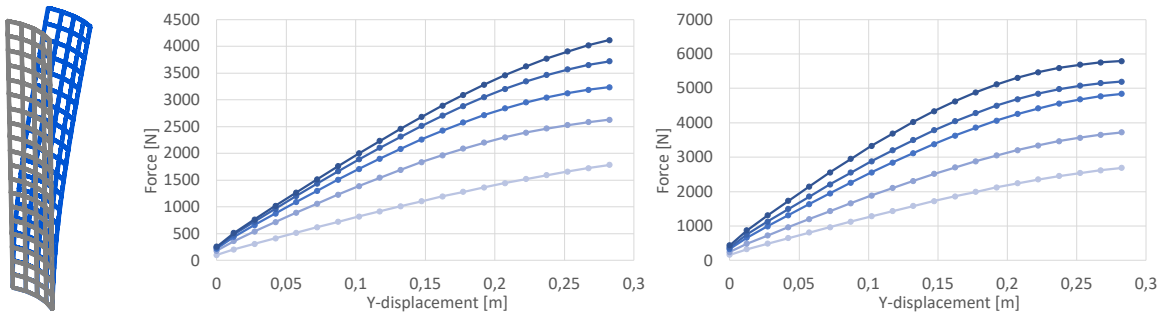

(a) Structure model. **(b)** Force deflection for varying values of V_{res}. **(c)** Force deflection for varying values of U_{res}.

Figure C.5: Model and force-deflection graphs of structure with beam-radius of 6mm, $\kappa = 5\text{m}^{-1}$, and varying values of U_{res} (figure C.5b) and V_{res} (figure C.5c).

C.3. Varying radius

For the exoskeleton A and exoskeleton B design, the moment-angle characteristic has been evaluated with varying radii. The moment-angle diagram of exoskeleton A is shown in figure C.6 and of exoskeleton B is shown in figure C.7. For exoskeleton A, the increase in radius mostly leads to a quantitative change in behavior. The stiffness of the structure does increase which leads to a higher reaction moment, but no qualtitative difference in structural behavior is found.

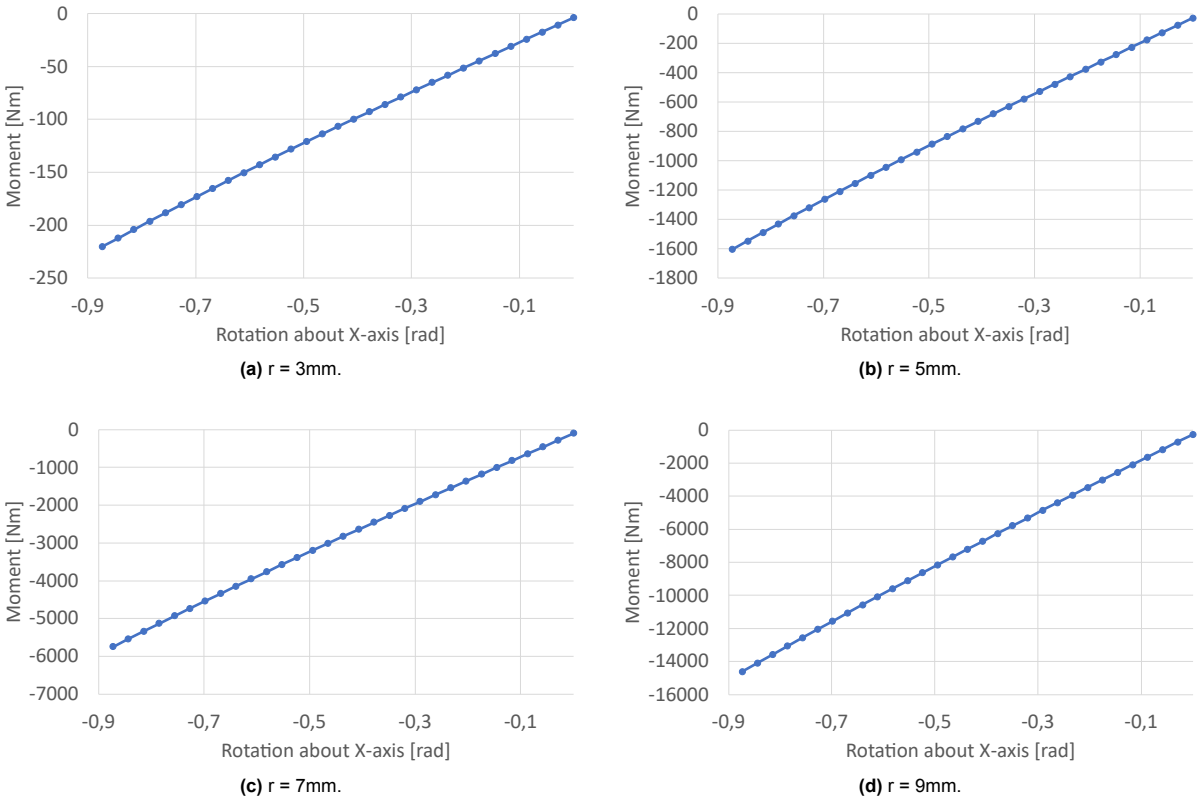

(a) r = 3mm.

(b) r = 5mm.

(c) r = 7mm.

(d) r = 9mm.

Figure C.6: Moment-angle graphs of exoskeleton A design with varying beam-radius ranging from 3mm to 9mm.

As can be seen in figure C.7, by increasing the radius, the structural behavior will change qualitatively. This can be seen by looking at the present peak at which the instability takes place. This peak becomes less pronounced when the radius is increased. This change is most likely induced by the structure being less prone to snap under compressive forces.

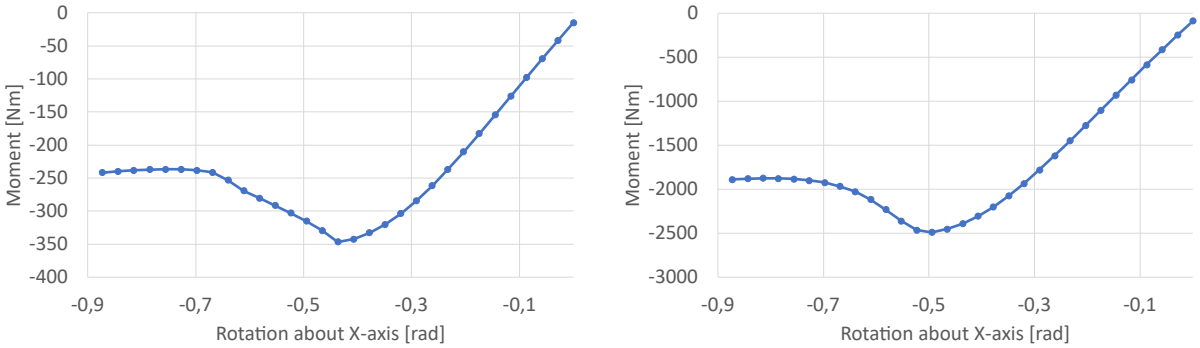

(a) r = 3mm.

(b) r = 5mm.

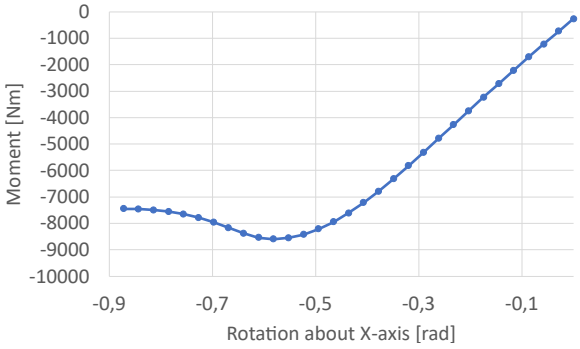

(c) r = 7mm.

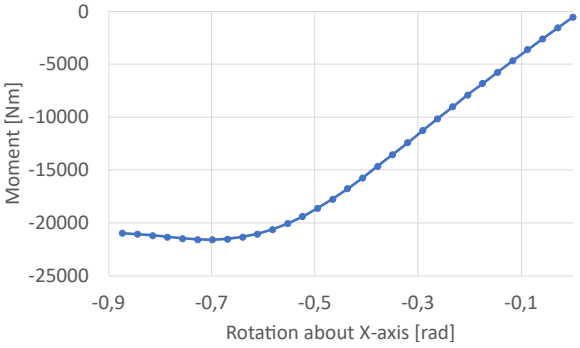

(d) r = 9mm.

Figure C.7: Moment-angle graphs of exoskeleton B design with varying beam-radius ranging from 3mm to 9mm.

D

Supplementary material: Exoskeleton design, production and validation.

D.1. Test models

In order to learn more about the mechanical behavior of the proposed structure, some experimental test models were 3D-printed and assembled. These models can be seen in figure D.1.

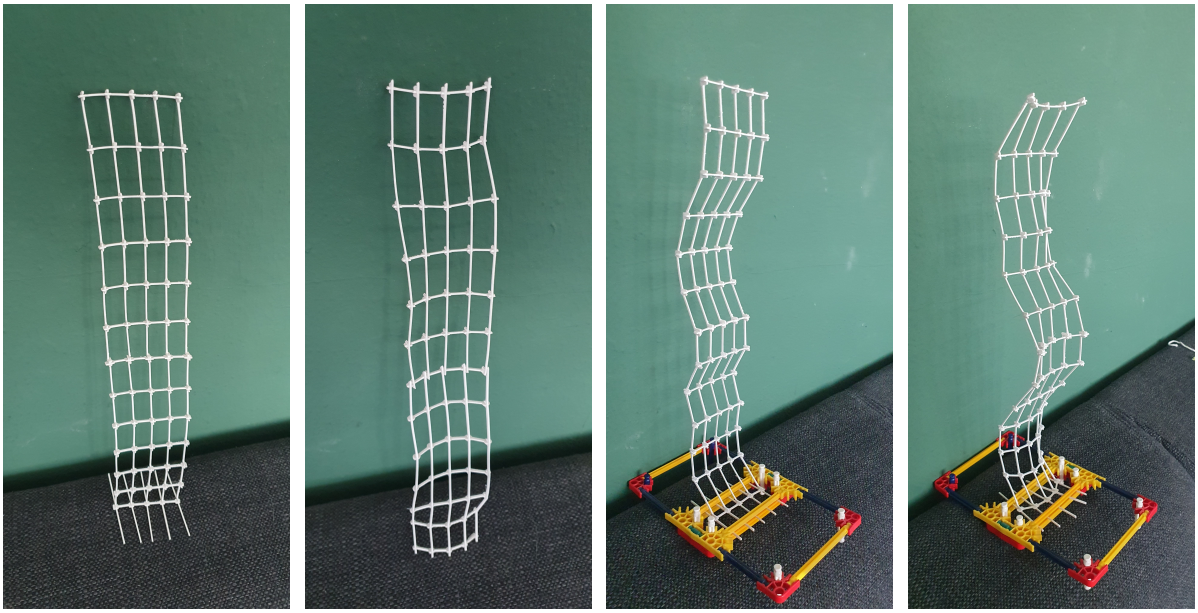

(a) Flat shaped structure.

(b) Arbitrary shaped structure.

(c) Structure with zero curvature and varying Y-offset.

(d) Structure with varying curvature and varying Y-offset.

Figure D.1: 3D-printed experimental models for verification of physical behavior which enables shape morphing.

D.2. Human back shape acquisition

The exoskeleton is designed for the author of this paper, and therefore the shapes of the authors back during deformation have been photographed and its contours have been traced as shown in figure D.2a. These contour lines have than manually been discretized to a set of nodal coordinates as shown in figure D.2b. These manually discretized coordinates are not equidistant from eachother, and thus have been used as input points for construction of a bezier curve that is thereafter discretized in order to acquire multiple sets of equidistantial nodes representing the objective shapes used in this paper.

D.3. Production method

Deciding on the correct production method is a big factor when determining material choice. Disregarding the elastic strain limit, the structure needs to be able to deform symmetrically as described in section 2. When using steel rods, the shape of the structure has to be created manually. This presents many challenges in conceiving a symmetric structure as well as constraining horizontal and vertical rods at nodal connection points. In figure D.2 the considered constraining methods for steel and PLA are shown. A drawback of using FDM technology to conceive a design is that for this structure, both the horizontal and vertical beam elements must be flat in order to fit on the printing plate. A similar rectangular design could also be considered by using laser cutting. This way, other materials such as titanium could be considered, using the same constraining method as in figure D.2d.

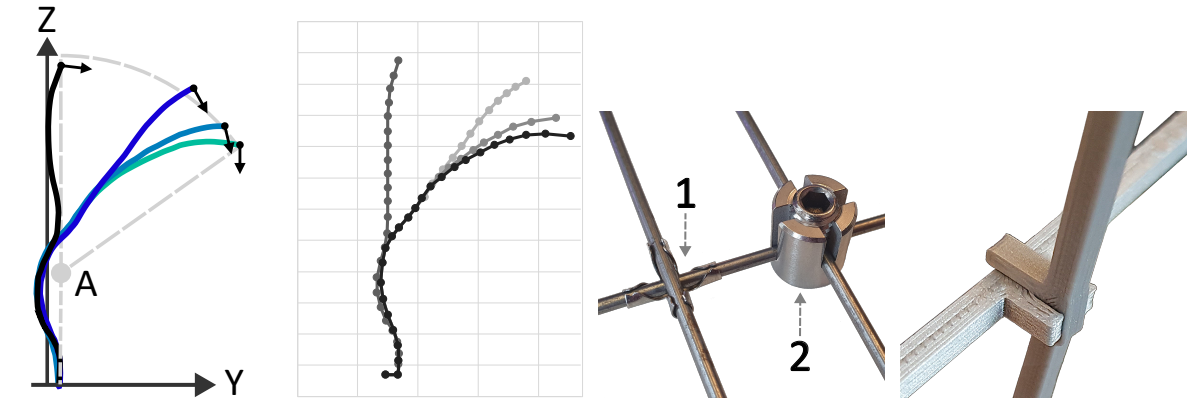

(a) Traced contour lines of back shape with approximate origin of rotation point A.

(b) Manually discretized nodal back coordinates.

(c) Constraint methods for connecting steel beams with angle clamp (1) and trellis clamp (2).

(d) Method of PLA beam connection using "U-fit" in combination with super glue.

Figure D.2: Deployed method of generating objective shapes representing human back with contour line tracing (figure D.2a) and manually discretized contour lines (figure D.2b) and evaluated material joining methods (figures D.2c and D.2d).

D.4. Exoskeleton production

The node coordinates of the structure are imported into Autodesk Inventor, and connected to form beams. Each horizontal and vertical U-fit (figure D.2d) is based on a single sketch, which is patterned to acquire every joint whole structure. Thereafter, beams are formed by sweeping a cross-section in parts along all nodes. In order for the exoskeleton design to be printable, the vertical beams had to be cut in pieces that fit on the printer bed. These vertical parts have been connected with small rectangular tubes to form the whole vertical structure. Every vertical connection and horizontal connection has been fixed with super glue.

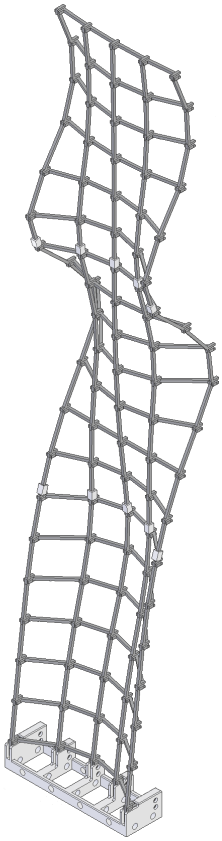

(a) Isometric view of 3D model made with Autodesk Inventor.

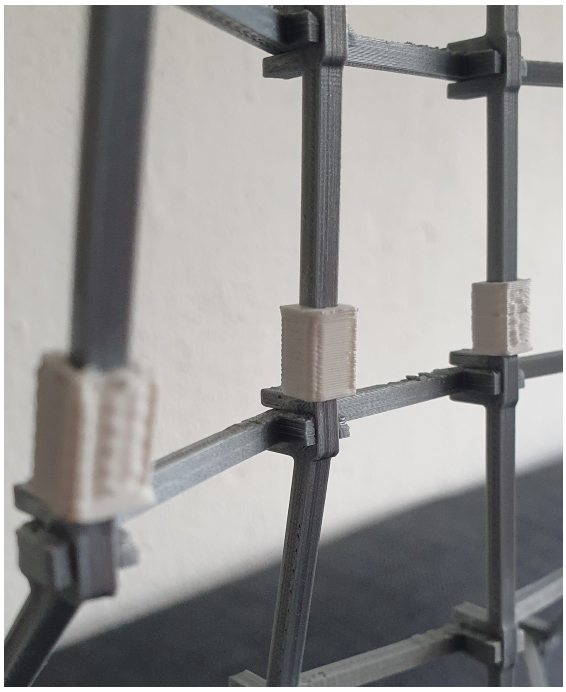

(b) Close-up of rectangular tube that connects vertical sections.

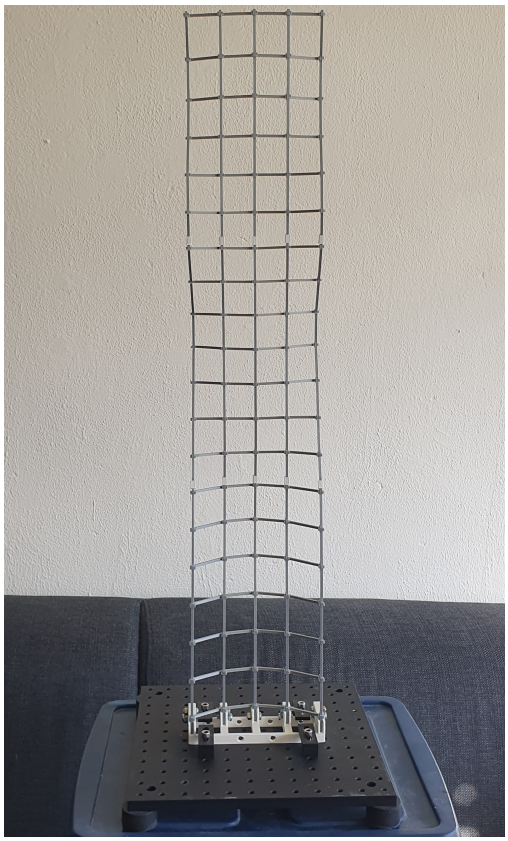

(c) Frontal view of the rectangular grid structure.

(d) Isometric view of exoskeleton prototype.

Figure D.3: Pictures of the rectangular grid exoskeleton prototype with 3D-model (figure D.3a), tube connector (figure D.3b), rectangular grid view (figure D.3c) and isometric view (figure D.3d).

E

Supplementary material: Induced strains

E.1. Simplified theoretical model

In order to make an assessment on what material to use for producing a prototype for exoskeleton usage, the present strains during deformation of the structure should be taken into account. The strains that occur during deformation can be approximated for the horizontal segments by simplifying their geometry to a smooth beam that may have an initial curvature K_1 and deforms to a final curvature K_2 as described in appendix E.1.

$$R_1 = \frac{1}{K_1} \tag{E.1a}$$

$$R_2 = \frac{1}{K_2} \tag{E.1b}$$

These curvatures relate to the radius of curvature as described in equation (E.1). By looking at the change in radius of curvature from R_1 to R_2, an estimation of the induced strain ϵ can be made, as described in equation (E.2).

$$\epsilon = r_f \frac{R_2 - R_1}{R_2 R_1} \tag{E.2}$$

The vertical resolution V_{res} for the generated designs is 20, and for these levels the induced strain will be evaluated.

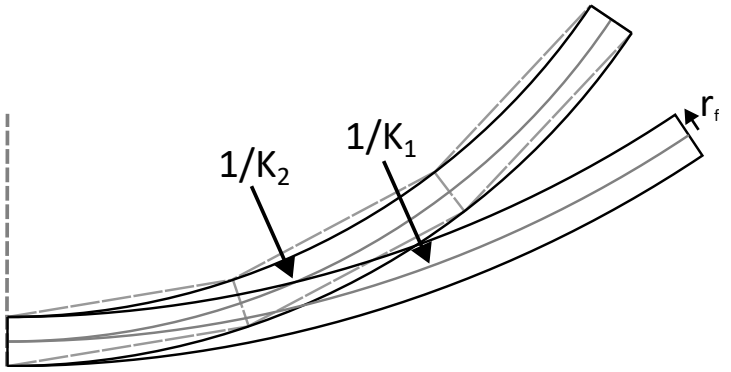

Figure E.1: Two beams with varying curvatures K (black), fiber distance r_f and discretized beam geometry (striped grey).

E.2. Results

Most steels have an elastic strain limit ranging from 0.2% to 0.6%. Commonly used plastics for 3D-printing such as PLA and PETG have higher strain limits ranging from 2% to 6%. When evaluating the induced strains in the designs from figures E.2a and E.2b, it is clear that steel is not a viable option when dealing with large deformations. For usage in exoskeletons, due to the large deformations in the structure another material that could be used for production could be titanium as the strain limit of this material can range from 0.5% to 2%. A rectangular grid model generation must then be used in order allow for production by laser-cutting.

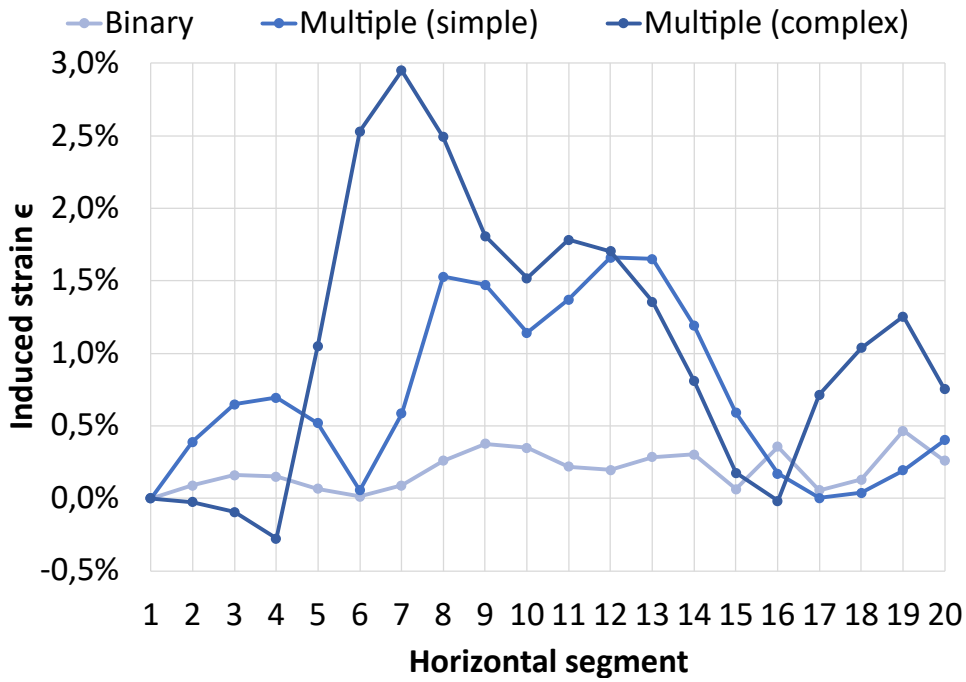

(a) Induced strains in horizontal segments due to structural deformation of binary shapes, multiple shapes (simple) and multiple shapes (complex) design.

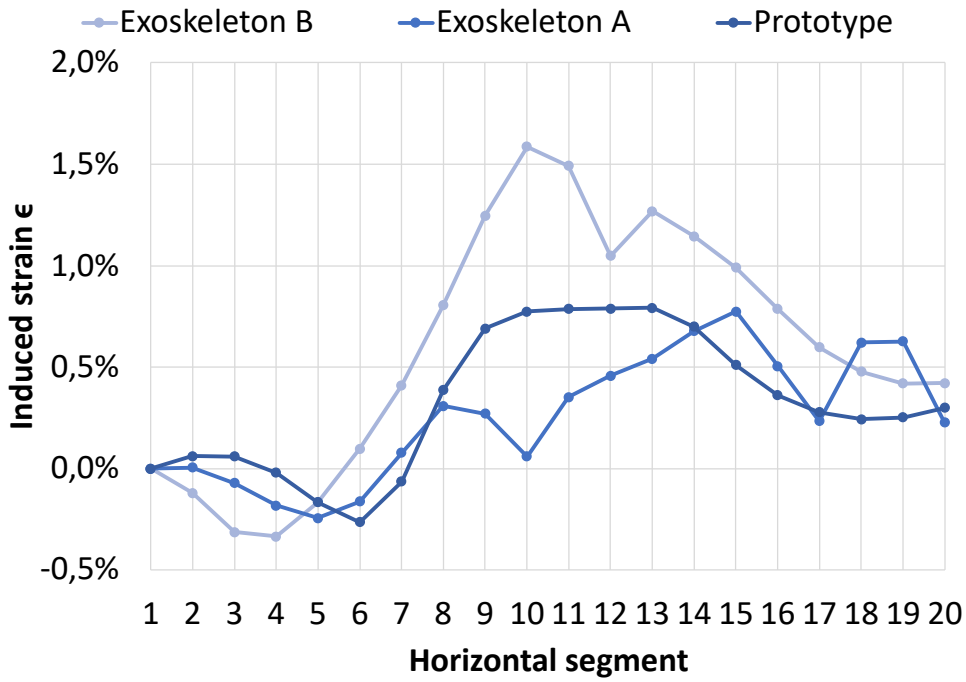

(b) Induced strains in horizontal segments due to structural deformation of the exoskeleton A, exoskeleton B and prototype design.

Figure E.2: Induced strains in demonstrative designs (figure E.2a) and exoskeleton designs (figure E.2b).

F

Supplementary material: Experimental validation

(a) Bellow for applying the angular displacement.

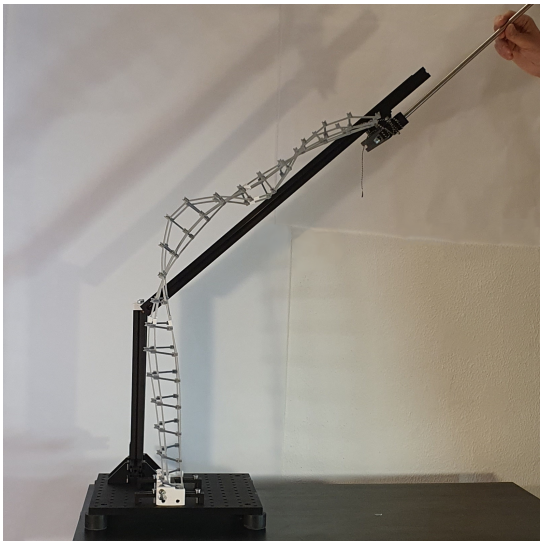

(b) Exoskeleton prototype measurement setup side view.

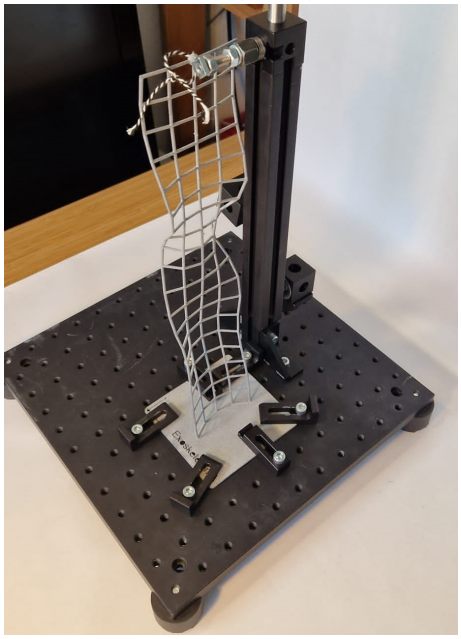

(c) Exoskeleton scale model at measurement setup

(d) Snap-through scale model exoskeleton at measurement setup.

(e) Exoskeleton prototype measurement setup.

Another image of the produced scale models is shown in figure F.2. In order to apply the rotational constraint for the multiple shapes (simple) design, a bellow has been constructed from a flexible electrical conduit with a custom 3D-printed adapter. By putting a hole in the adapter design, and drilling one in

the conduit, they can be fixed together with a tie-wrap. The bellow is shown in figure F.1a. The physical setup of the simplified back model can be seen at full-scale in figure F.1b as well as a smaller version in figures F.1c and F.1e. Several Thorlabs components such as a base plate and beams are used, in combination with some short wire to pull the exoskeletons and a 3D-printed hinge for figure F.1b.

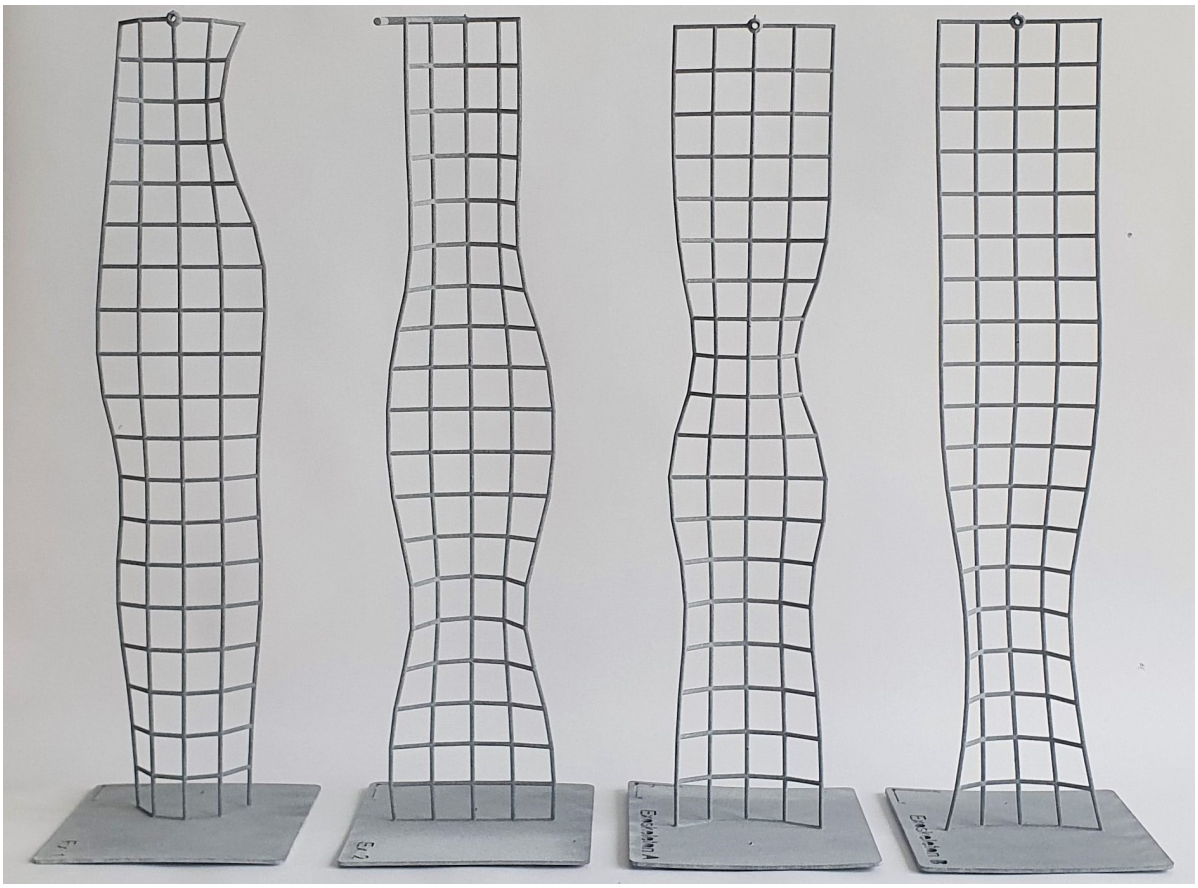

Figure F.2: Produced scale models with Multi-Jet Fusion production method.

G

Supplementary material: Code diagram

In order to provide an overview of the conducted steps in the proposed design method, a code diagram has been generated. This diagram gives a description of the most important steps during initialization (figure G.1a), random search (figure G.2a) and minimization (figure G.2b) and comes with a legend (figure G.1b).

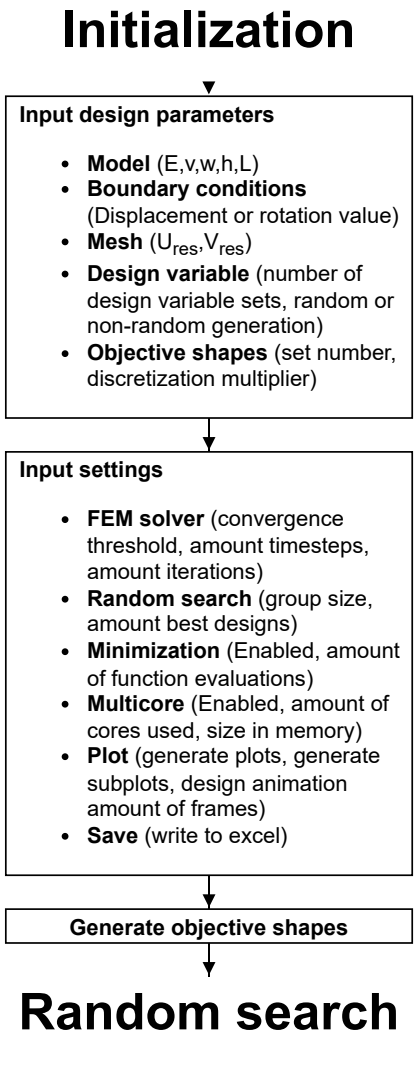

(a) Initialization step of design algorithm.

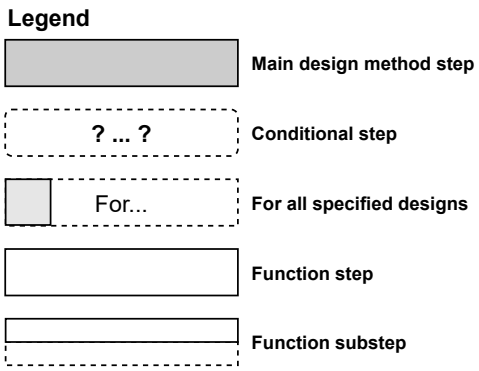

(b) Legend describing used blocks in code diagram.

Figure G.1: Simplified diagram of initialization of design algorithm and corresponding steps represented by rows (figure G.1a) and corresponding legend (figure G.1b) on right.

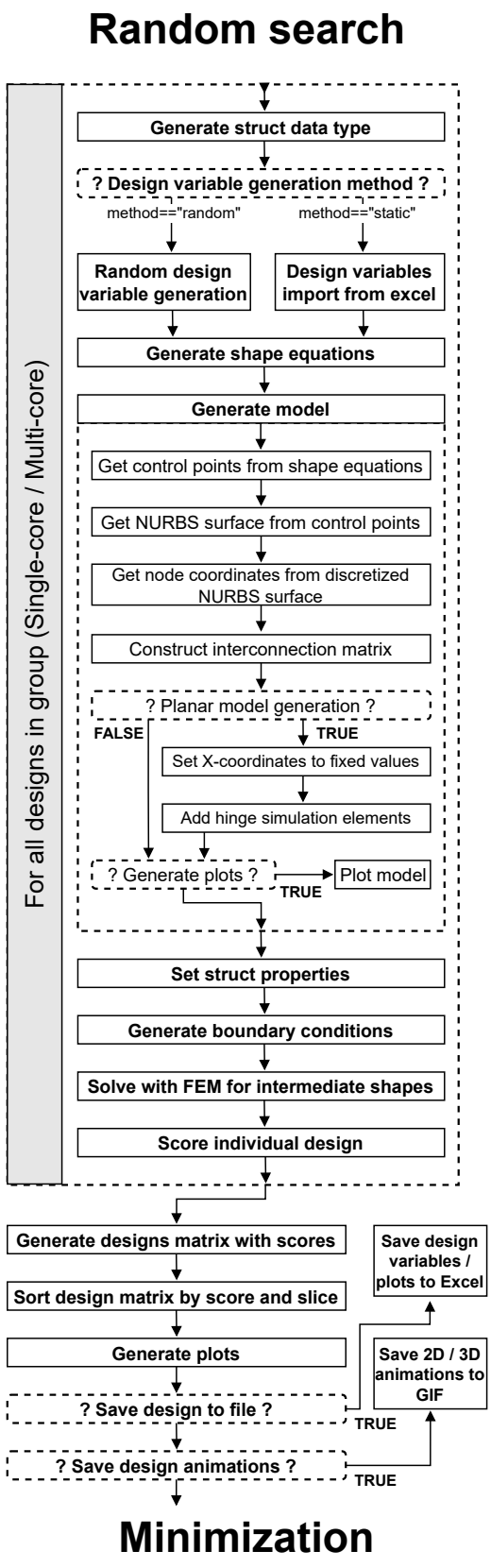

(a) Initialization step of design algorithm.

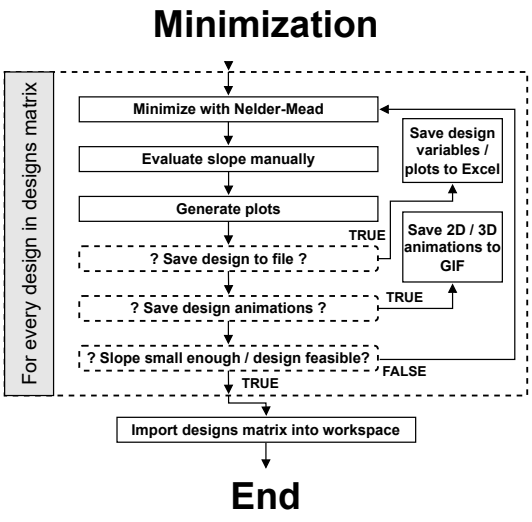

(b) Legend describing used blocks in code diagram.

Figure G.2: Simplified diagram of random search step (figure G.2a) and minimization step (figure G.2b) of design algorithm and corresponding steps represented by rows.

H

Supplementary material: Multi-threading

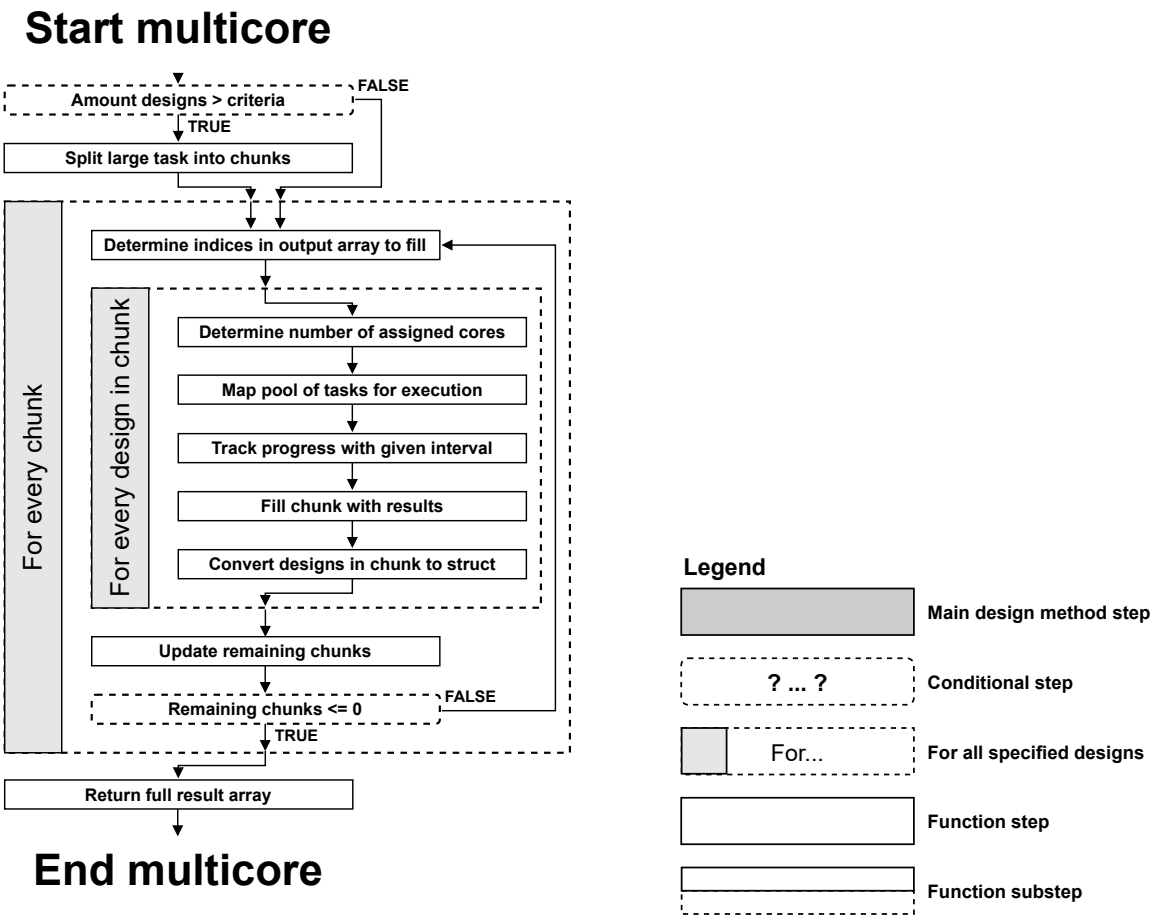

(a) Multi-thread function.

(b) Legend describing used blocks in multi-thread diagram.

Figure H.1: Description of multi-thread function steps (figure H.1a) and corresponding legend(figure H.1b).

H.1. Parallelism

In order to realize a better understanding of the Finite Element Method as well as to enable the full design method to work in python, the FEM code has been converted from it's existing version based on MATLAB and C++ to a fully Python-based one. An advantage of this translation is that the Python-based code has been tailored towards parallelism. The existing code utilized a C++ multi-thread-accelerated construction of the stiffness matrix for the whole structure. While this is desirable for evaluating a single structure once or multiple times, when evaluating large amounts of designs in parallel it is not desirable to utilize all CPU threads for every design. Rather, a single-thread-based approach for design evaluation allows every thread to evaluate a single design and thus it can be easily scaled up. For implementation of this multi-thread based-approach, the *multiprocessing* python library was used. A general description of the steps of the multi-threaded function is given in figure H.1.

H.2. Chunk size

The multi-threaded function has a parameter known as the chunk size, which determines the size of a task to be loaded into memory. It is crucial to manage the system memory when using this parameter since loading the full task into memory can cause memory issues. Therefore, limiting the memory usage makes sense.

H.3. Memory adress referencing

Another important consideration of multi-threaded execution is that each assigned thread operates in an isolated environment. As a result, any struct datatypes used and stored within this environment cannot be accessed from outside. To avoid referencing a memory address in the multi-thread isolated environment, all struct datatype models are converted to a nested list before being passed as an output argument of the multi-thread function.

H.4. Conclusion

A drawback of this introduced parallelism is that for the minimization step, the evaluation of designs is in single core. Due to time constraints for the project, this minimization process is not enhanced for parallel execution and as a result, it runs single-threaded. Thus, the task takes longer to execute for a single design as compared to the original MATLAB code. The introduced advantage is however, that a parallel random search can be conducted.